Perovskite solar cells by vapor deposition based and assisted methods

Perovskite Solar Cells by Vapor Deposition Based and Assisted Methods

Yan Jiang,[1,*] Sisi He,[2] Longbin Qiu,[3,*] Yixin Zhao,[4, a)] and Yabing Qi[5,*]

[1] *Energy Materials and Optoelectronics Unit, Songshan Lake Materials Laboratory, Dongguan, Guangdong, 523808, China*

[2] *Flexible Printed Electronics Technology Center, School of Science, Harbin Institute of Technology Shenzhen, Nanshan District, Shenzhen, Guangdong Province 518055, China*

[3] *Department of Mechanical and Energy Engineering, Southern University of Science and Technology, Shenzhen, 518055, China*

[4] *School of Environmental Science and Engineering, Frontiers Science Center for Transformative Molecules, Shanghai Jiao Tong University, Shanghai, 200240 China*

[5] *Energy Materials and Surface Sciences Unit (EMSSU), Okinawa Institute of Science and Technology Graduate University (OIST), 1919-1 Tancha, Onna-son, Okinawa, 904-0495, Japan*

(*Corresponding authors: jiangyan@sslab.org.cn; qiulb@sustech.edu.cn; Yabing.Qi@OIST.jp)

ABSTRACT

Metal halide perovskite solar cells have made significant breakthroughs in power conversion efficiency and operational stability in the last decade, thanks to the advancement of perovskite deposition methods. Solution-based methods have been intensively investigated and deliver record efficiencies. On the other hand, vapor deposition-based and assisted methods are less studied in the early years but have received more attention recently due to their great potential towards large-area solar module manufacturing and high batch-to-batch reproducibility. Besides, an in-depth understanding of perovskite crystallization kinetics during the vapor deposition based and assisted process allows increasing perovskite deposition rate and enhancing perovskite electronic quality. In this review, the advances in vapor-based and assisted methods for the fabrication of perovskite solar cells are introduced. In addition, the quality of the perovskite layers (i.e., morphology, crystallinity, defect chemistry, carrier lifetime) fabricated by different methods are compared. The limitations of state-of-the-art vapor-deposited perovskite layers are discussed. Finally, insights into the engineering of vapor deposition based and assisted perovskite layers towards efficient and stable perovskite solar cells and modules are provided.

TABLE OF CONTENTS

I. INTRODUCTION

Global warming, air pollution and the increasing energy demand indicate the urgent necessity of developing abundant clean renewable energy. Photovoltaic (PV) is a clean energy conversion process and will meet the needs of over 12 terawatt energy requirement by 2050.[1] Perovskite solar cells (PSCs), using metal halide perovskites as absorbers, are a new class of thin-film PV technology.[2] In 2009 Miyasaka et al. reported a mesoporous-structured PSC for the first time with a power conversion efficiency (PCE) of 3.8%.[3] Motivated by this

proof-of-concept study, a series of experiments and density functional theory (DFT) calculations were carried out, revealing that perovskites are ideal PV absorbers with high absorption coefficient,[4-7] tunable bandgap,[8] long carrier diffusion length[9-12] and high tolerance of defects (low density of deep level defects).[13-16] In 2021, PSCs have demonstrated a certified PCE of 25.7% on the lab scale (~0.1 cm^2), surpassing the other thin-film PVs and comparable with crystalline silicon PV.[17] A carbon-based 2D/3D perovskite solar module shows negligible PCE decay over 10000 h under continuous 1-sun illumination, equal to operation for 4 hours every day under standard illumination for about 6.8 years.[18] Besides, technology commercialization is on the way. Oxford PV, Microquanta Semiconductor, Toshiba, Panasonic and Solaronix are pioneer companies devoted to perovskite solar module manufacturing, to name a few. On November 2021, Microquanta Semiconductor reported a new certified record high efficiency of 21.4% on a mini-module (19.32 cm$_2$).[19] On July 2021, Oxford PV announced the completion of its perovskite-on-silicon tandem solar cell manufacturing line with an annual target manufacturing capacity of 100 MW.[20]

The perovskite layer is the key component in a PSC. Morphology, thickness, crystallinity, stoichiometry and defect level/density of perovskite layer determine photon absorption, charge transport and recombination kinetics, and ion migration activation energy, which all have a

significant impact on solar cell PCE and stability.[21-23] In the last decade, great effort has been made in the development of deposition methods to obtain high-quality perovskite absorbers.[24] Solution-based methods, such as spin-coating,[25] spray-coating,[26-28] blade-coating,[29-30] slot-die coating,[31-32] etc. have been intensively investigated. Taking advantage of the advanced strategies such as anti-solvent dripping,[33] solvent engineering,[34] solvent annealing,[35] hot-casting,[36] etc. record efficiencies of solution-processed perovskite solar cells are continuously rising for both small cells and modules (Figure 1). On the other hand, vapor deposition based and assisted (VDBA) methods were relatively less studied in the initial years but have received more attention recently. Vapor deposition-based methods include thermal evaporation,[7] chemical vapor deposition[37-38] and close-space sublimation[39] etc. in which perovskite absorbers are fabricated in a chamber or a furnace under vacuum condition without involving any solvent. Vapor deposition-assisted methods are a combination of vapor and solution methods when the crystallization process is usually conducted on a hotplate and at low or ambient pressure. An in-depth understanding of perovskite crystallization kinetics during the VDBA processes allows increasing perovskite deposition rate and enhancing perovskite electronic quality, resulting in vapor-processed perovskite solar cells that are fast catching up with the solution-processed perovskite solar cells (Figure 1).
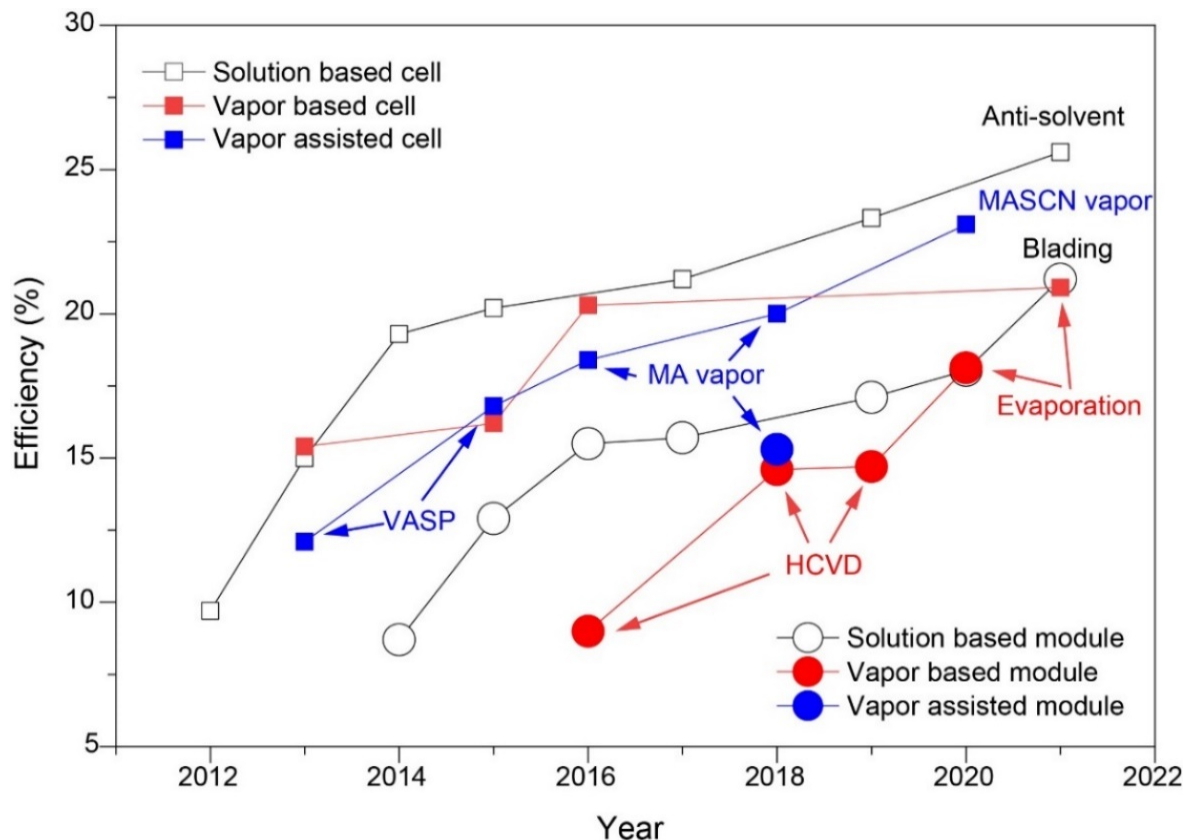

Figure 1. Efficiency evolution of perovskite solar cells and modules (with an area over 10 cm^2). The data points are collected from published papers on solution-based cells,[40-45] vapor-based cells,[7, 39, 46-47] vapor-assisted cells,[25, 48-51] solution-based modules,[52-57] vapor-based modules[58-61] and vapor-assisted modules.[50]

VDBA methods offer several unique advantages. (I) No or less solvent concerns. Solvents such as N,N′-dimethylformamide (DMF), dimethyl sulfoxide (DMSO), γ-butyrolactone (GBL) and anti-solvent such as toluene (TL), chlorobenzene (CB), and diethyl ether (DE) are mostly used in research labs to prepare perovskite layers via solution processing. However, toxicity concerns and handling issues pose a great hindrance for large-scale manufacturing. Besides, a solvent with a high boiling point can leave residues in perovskite even after annealing, causing instability risks.[62-63] In the case of VDBA methods, no solvent (vapor based) or less solvent (vapor assisted) is used during perovskite deposition, solving these solvent-related issues. (II) Processing up-scalability. Molecular diffusion rates of reactants (i.e., organic halides) are significantly faster in a vapor phase (diffusion or pressure-driven) compared to a liquid phase (external force driven). Organic halide vapors with uniform partial pressures are created in the reaction chamber during a VDBA process, resulting in perovskite films with large-area uniformity and high batch-to-batch reproducibility.[64-67] (III) Ease integration with existing thin-film PV manufacturing lines. VDBA methods such as thermal evaporation, plasma-enhanced chemical vapor deposition (PECVD), have been widely applied in fabricating absorbers of other thin-film PVs, i.e., a-silicon,[68-69] CIGS,[70] CdTe.[71] These manufacturing lines, with necessary upgrading, may be suitable for PSC manufacturing. The knowledge gained in thin-film PVs can also provide valuable insights for technology commercialization of PSCs fabricated by the VDBA methods. For example, the exact manufacturing cost via different VDBA methods may vary but are similar compared with solution-based methods, as reported in our recent review.[72]

II. PROGRESS IN VAPOR DEPOSITION-BASED PEROVSKITE SOLAR CELL

Vapor deposition-based methods are a mature technique widely applied in the semiconductor industry for optoelectronic applications, i.e., solar cells, organic light-emitting diodes (OLEDs), lasers, etc. Vapor deposited perovskite film ($(RNH_3)_2PbI_4$) was first reported by Era et al. in 1997 with a history of over 2 decades.[73] In view of the deposition pressure, vapor deposition-based methods can be divided into two groups, i.e., high vacuum deposition techniques (e.g., thermal evaporation) and low vacuum deposition techniques (e.g., chemical vapor deposition and close space sublimation).

A. High vacuum deposition techniques

1. Co-evaporation method

In 2013, Snaith et al. reported a dual-source co-evaporation technique to deposit a $CH_3NH_3PbI_{3-x}Cl_x$ perovskite film at a pressure below 10^{-5} mbar (**Figure 2a**).[7] CH_3NH_3I and $PbCl_2$ were simultaneously sublimated for the formation of perovskite and the substrate holder was water-cooled and rotated to improve uniformity. The deposition rates of each source and composition of the final perovskite film were optimized, which resulted in a perovskite film with high purity and superior uniform thickness (**Figure 2d**). A planar-structured PSC showed a PCE of over 15%. A key challenge in co-evaporation of perovskites lays in calibration and controlling the evaporation rate of organic halide sources. Qi et al. optimized the geometry of a homemade instrumentation that allowed monitoring the CH_3NH_3I vapor partial pressure inside the vacuum chamber. Highly uniform perovskite films were fabricated using the hybrid deposition method, which delivered efficiencies of 9.86% in PSCs in 2014,[74] and 11.48% in 2015 with the advancement of perovskite film morphology and roughness.[75]

In 2016, Bolink et al. developed a series of intrinsic (i.e., N4,N4,N400,N400-tetra([1,10-biphenyl]-4-yl)-[1,10:40,100-terphenyl]-4,400-diamine (TaTm), C_{60}) and doped organic charge transport molecules (TaTm:F6-TCNNQ, C_{60}:Phlm) that are suitable for vacuum deposition. They for the first time demonstrated fully vapor processed PSCs with a PCE of 16.5% in a p-i-n configuration and 20% in an n-i-p configuration, respectively (**Figure 2e**).[46] These devices had an operational T_{80} lifetime of around a week. Later on, they showed that mixed cations/anions organic-inorganic hybrid perovskites ($FA_xMA_yCs_{1-x-y}PbI_zBr_{3-z}$)[76] and inorganic perovskites ($CsPbI_xBr_{3-x}$)[77] could also be deposited via the co-deposition approach by precise regulating sublimation rate of multiple sources (**Figures 2b-c**). Liu et al. reported that the perovskite optoelectronic property and PSC stability could be enhanced by Cs substitution via a co-deposition process.[78] In 2021, Albrecht et al. used co-evaporation method to deposit $FA_xMA_{1-x}PbI_3$ and achieved a high PCE of 20.4%. The method showed good compatibility in fabricating monolithic fully textured perovskite/silicon tandems with a PCE of 24.6%.[79] Two-dimensional perovskites exhibited higher ion migration activation energy compared to three-dimensional perovskites and might hold the key to solving the solar cell instability issue. In 2020, Bolink et al. developed a dual-source vacuum co-deposition technique for 2D perovskite i.e., PEA_2PbX_4 (PEA = phenethylammonium and X = I^-, Br^-, or a combination of both).[80] Low bandgap tin-lead mixed perovskites (Eg < 1.4 eV) can be used as bottom cells in tandem devices and have obtained considerable research interests. Solution-processed tin-lead mixed perovskites rely on the use of a small amount of SnF_2 to reduce the formation of Sn^{4+}, which is technically challenging to control via vacuum deposition. In 2020, Bolink et al. reported vacuum co-deposition of $MA_{0.9}Cs_{0.1}Sn_{0.25}Pb_{0.75}I_3$ without the need of SnF_2. They found that the ratio between the monovalent (MA^+, Cs^+) and divalent metal cation (Sn^{2+}, Pb^{2+}) determines the optoelectronic properties. Precisely controlling the ratio resulted in a $MA_{0.9}Cs_{0.1}Sn_{0.25}Pb_{0.75}I_3$ PSC with PCE reaching 8.89%.[81] To demonstrate the superiority of this technique toward up-scalability, Bruno et al. prepared co-evaporated $MAPbI_3$ perovskite solar modules with an active area of 21 cm^2 and PCE of 18.13%
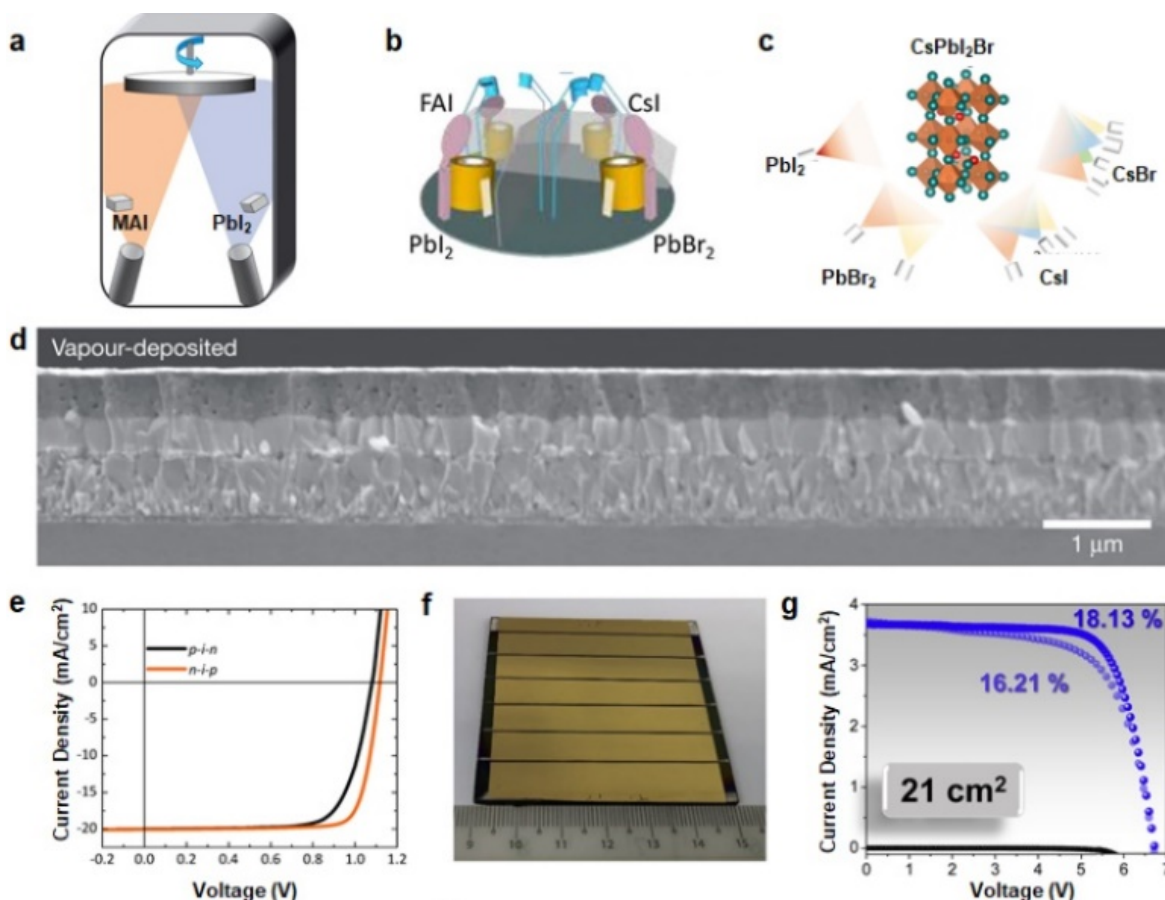
Figure 2. Co-evaporation to deposit perovskite films. Illustration of **(a)** the dual-source and **(b-c)** multiple-source vacuum deposition instrument. **(d)** Cross-section SEM image of a co-evaporation deposited perovskite solar cell. **(e)** Current-voltage characteristics of co-evaporation deposited PSCs with the n-i-p and p-i-n configurations. **(f)** A photograph of co-evaporation deposited perovskite solar module and **(g)** the current-voltage characteristics. (a, d) Reproduced with permission from Nature 501, 395 (2013). Copyright 2013 Springer Nature. (b) Reproduced with permission from ACS Energy Lett. 6, 827 (2021). Copyright 2021 American Chemical Society. (c) Reproduced with permission from Chem. Mater. 32, 8641-8652 (2020). Copyright 2020 American Chemical Society. (e) Reproduced with permission from Energy Environ. Sci. 9, 3456 (2016). Copyright 2018 the Royal Society of Chemistry. (f-g) Reproduced with permission from Joule 4, 1035 (2020). Copyright 2020 Elsevier Inc.

(**Figures 2f** and **g**).[61] The unencapsulated PSCs retained 90% of their initial PCE under 1-sun illumination condition for more than 100 h. The results are quite exciting and could promote more research interest in the further development of this technique.

2. Sequential deposition method

The co-evaporation technique relies on simultaneously controlling the deposition rates of multiple evaporation sources to obtain a perovskite film with an intended composition or composition profile. As an alternative, the sequential deposition technique allows deposition of a perovskite film in a layer-by-layer manner, which avoids the difficulty in simultaneously controlling the deposition rates of precursors and simplifies the instrumentation design. In 2014, Lin et al. developed a two step-sequential deposition technique for MAPbI$_3$, with PbCl$_2$ first deposited on the ITO/PEDOT:PSS substrate followed by

deposition of MAI (**Figure 3a**).[82] The reaction kinetics were investigated by tuning the substrate temperature, resulting in a pin-hole free perovskite film with complete conversion (**Figure 3b**). When deposited at 75 °C, the MAPbI$_3$ PSC delivered a PCE of 15.4% and external quantum efficiency (EQE) of 80% between 450 and 750 nm wavelength range. Liu et al. used a similar method but with multiple deposition cycles to deposit MAPbI$_3$ and obtained an improved PCE of 16.03%.[83] Qi et al. applied the method for deposition of tin-based perovskite (i.e., MASnBr$_3$) for PV application. The formation of MASnBr$_3$ was confirmed by XRD and UV-Vis measurements. Based on the XPS analyses, MASnBr$_3$ films prepared by sequential evaporation showed much less an effect of oxidized Sn species than those prepared by co-evaporation.[84] Fan et al. prepared mixed cation and mixed halide perovskites via sequential evaporation. Optimization of the cation ratios and development of vapor-deposited charge transport layers allowed them to fabricate an all-vacuum-deposited

PSC with a PCE of up to 15.14%.[85] Liu et al. recently reported a high-throughput large-area vacuum deposition method for the preparation of highly uniform perovskite films on rigid and flexible substrates (**Figures 3c** and **d**).[47] PbI_2, FAI and CsI were evaporated in sequence on the FTO/TiO_2 substrates, followed by a vacuum annealing step. They showed that temperature of vacuum annealing was critical in regulating crystal domain size, density of defects and charge transfer dynamics. At a low annealing temperature, FAI reacted with the upper portion of the PbI_2 layer but partially with the lower portion (could be diffusion-limited). At a high annealing temperature, decomposition of perovskite started at the grain boundary, causing the formation of PbI_2. These PbI_2 species served as carrier blocking layers hindering the charge transport. By engineering the strain and tuning the crystallization temperature of perovskite, they reported sequentially deposited PSCs $(FTO/TiO_2/FA_xCs_{1-x}PbI_3/Spiro-MeOTAD/Au)$ with an efficiency of 21.32% (**Figures 3e** and **f**), a record high efficiency obtained so far for vapor-based deposition techniques. Furthermore, they showed that the long-term environmental stability could be significantly improved by substitution of spiro-MeOTAD with an NPB (N,N0-Di(1-naphthyl)-N,N0-diphenyl-(1,10-biphenyl)-4,40-diamine)/MoO_x bilayer (**Figure 3g**). **Table 1** has summarized the PCE and lifetime evolution for the PSCs fabricated by various high vacuum deposition techniques.
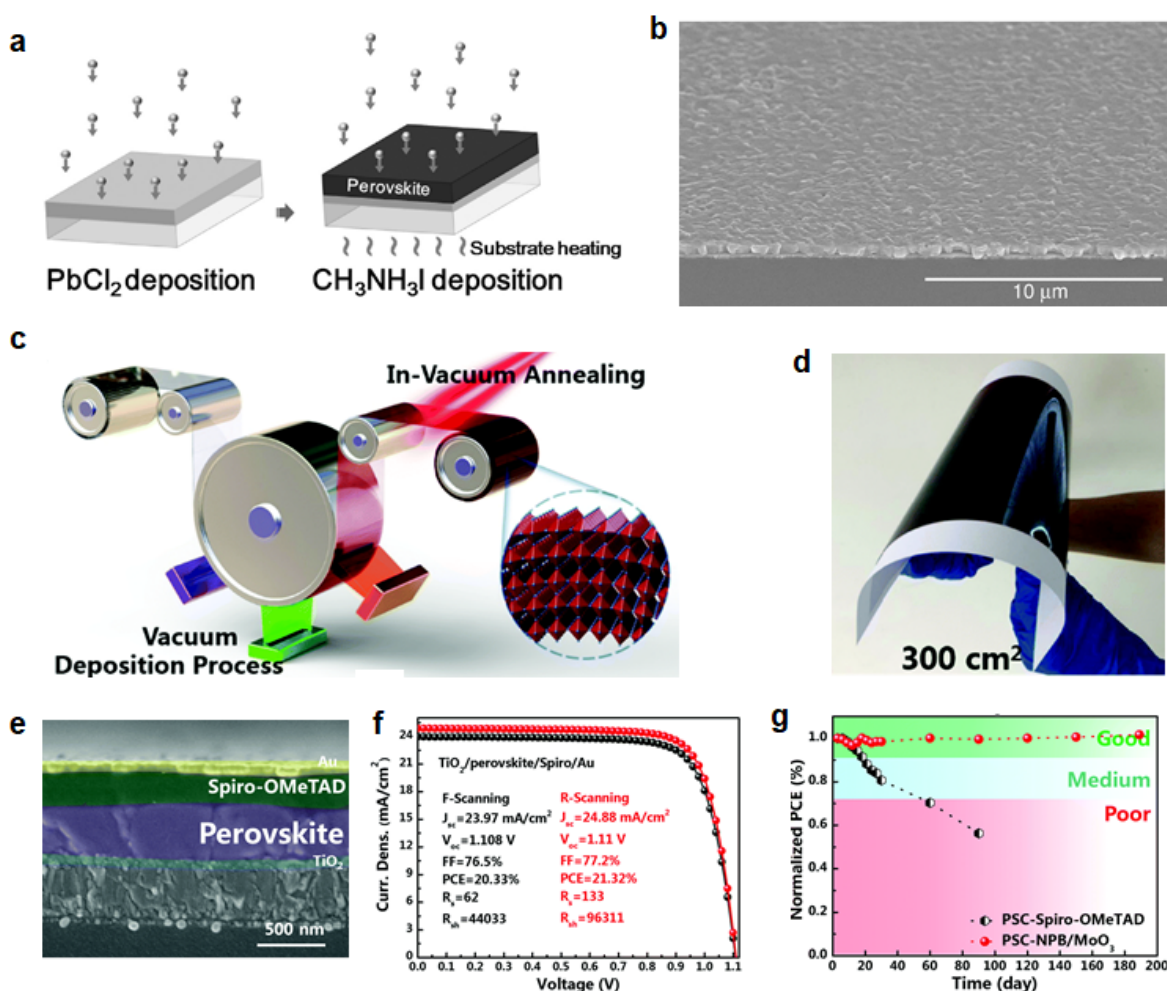
Figure 3. Sequential evaporation to deposit perovskite films. (a) Schematic illustration of a two-step sequential deposition method. **(b)** SEM image of the $MAPbI_3$ layer prepared by a two-step sequential deposition. **(c)** Illustration of an all-vacuum deposition system and **(d)** a photograph of the as-prepared perovskite film on a flexible substrate. **(e)** Cross-section SEM image, **(f)** the current-voltage characteristics, and **(g)** stability of the PSCs. (a-b) Reproduced with permission from Adv. Mater. 26, 6647 (2014). Copyright 2014 Wiley-VCH. (c-g) Reproduced with permission from Energy Environ. Sci. 14, 3035 (2021). Copyright 2021 the Royal Society of Chemistry.

TABLE 1. Summary of perovskite solar cells by high vacuum deposition techniques.

Method	Device structure	V_{oc} (V)	Jsc (mA cm^{-2})	FF (%)	η (%)	Area (cm^2)	Lifetime (h)	Year	Reference

Method	Device structure	V_{oc}	J_{sc}	FF	PCE	Area	Stability	Year	Ref
Co-evaporation	FTO/c-TiO$_2$/Perovskite/Spiro-MeOTAD/Ag	1.07	21.5	67	15.4	0.076	NA	2013	7
Co-evaporation	ITO/PEDOT:PSS/polyTPD/MAPbI$_3$/PCBM/3TPYMB/Au	1.09	18.2	75	14.8	0.065	NA	2014	86
Co-evaporation	ITO/PEDOT:PSS/polyTPD/MAPbI$_3$/PCBM/3TPYMB/Au	1.07	17.9	57	10.9	0.95	NA	2014	86
Co-evaporation	ITO/C$_{60}$:Phlm/C$_{60}$/MAPbI$_3$/TaTm/TaTm:F6-TCNNQ/Ag	1.14	22.08	80.5	20.3	0.1	7 days[d]	2016	46
Co-evaporation	FTO/TiO$_2$/MA$_x$Cs$_{1-x}$PbI$_3$/Spiro-MeOTAD/Au	1.10	23.17	79	20.13	0.09	10[d]	2017	78
Co-evaporation	ITO/C$_{60}$:Phlm/C$_{60}$/MAPb(Br$_{0.2}$I$_{0.8}$)$_3$/TaTm/TaTm:F$_6$-TCNNQ/Au	1.119	17.3	82.3	15.9	-	NA	2018	87
Co-evaporation	ITO/C$_{60}$:Phlm/C$_{60}$/Cs$_{0.5}$FA$_{0.4}$MA$_{0.1}$Pb(I$_3$Br$_{0.17}$)$_3$/TaTm/TaTm:F$_6$-TCNNQ/Au	1.146	17.0	82	16.0	-	120[d]	2018	88
Co-evaporation	ITO/MoO$_3$/TaTm/CsPbI$_2$Br/C$_{60}$/BCP/Ag	0.958	14.3	73.1	10	0.065	NA	2020	77
Co-evaporation	FTO/TiO$_2$/SnO$_2$/PCBM/MAPbI$_3$/Spiro-MeOTAD/Au	1.12	23.3	77.7	20.28	0.1	3[d]; 60 days[c]	2020	61
Co-evaporation	FTO/TiO$_2$/SnO$_2$/PCBM/MAPbI$_3$/Spiro-MeOTAD/Au	6.71	3.68	73.44	18.13	21[a]	NA	2020	61
Co-evaporation	ITO/MoO$_3$/TaTm/FA$_{(1-n)}$Cs$_n$Pb(I$_{1-x}$Br$_x$)$_3$/C$_{60}$/BCP/Ag	1.184	18.0	79	16.8	-	14 days[d]; 21 days[c]	2021	76
Co-evaporation	ITO/MoO$_3$/PTAA/FAPb$_{0.5}$Sn$_{0.5}$I$_3$/C$_{60}$/BCP/Ag	0.72	24.5	79.3	13.98	0.01	NA	2020	89
Co-evaporation	ITO/MeO−2PACz/FA$_x$MA$_{1-x}$PbI$_3$/C$_{60}$/BCP/Cu	1.05	25.70	75.91	20.4	0.16	1000[d]	2021	79
Hybrid deposition	FTO/c-TiO$_2$/MAPbI$_3$/Spiro-MeOTAD/Ag	1.09	16.98	53.49	9.86	0.05	NA	2014	74
Hybrid deposition	FTO/c-TiO$_2$/MAPbI$_3$/Spiro-MeOTAD/Au	1.098	19.92	52.44	11.48	0.06	NA	2015	75
Hybrid deposition	FTO/C$_{60}$/MAPbI$_3$/Spiro-MeOTAD/Au	1.10	18.9	75.4	15.7	0.08	NA	2016	90
Vapor sequential deposition	ITO/PEDOT:PSS/MAPbI$_{3-x}$Cl$_x$/C$_{60}$/Bphen/Ca/Ag	1.02	20.9	72.2	15.4	0.05	NA	2014	82
Vapor sequential deposition	FTO/c-TiO$_2$/MAPbI$_3$/Spiro-MeOTAD/Au	1.00	22.27	72	16.03	0.071	60 days[c]	2015	83
Vapor sequential deposition	FTO/c-TiO$_2$/MASnBr$_3$/Spiro-MeOTAD/Au	0.498	4.27	49.1	1.12	-	NA	2016	84
Vapor sequential deposition	FTO/c-TiO$_2$/CsPbBr$_3$/CuPc/C	1.328	7.59	75.2	7.58	0.09	1000[c]	2019	91
Vapor sequential deposition	FTO/c-TiO$_2$/FA$_x$MA$_{1-x}$PbI$_3$/Spiro-MeOTAD/Au	0.98	22.4	73	15.8	0.09	NA	2019	92
Vapor sequential deposition	FTO/c-TiO$_2$/FA$_x$MA$_{1-x}$PbI$_3$/CuPc/Au	1.02	19.16	77.3	15.14	-	240[c]	2019	85
Vapor sequential deposition	FTO/c-TiO$_2$/CsPbBr$_3$/C	1.42	6.49	79	7.22	0.16	30 days[c]	2020	93
Vapor sequential deposition	FTO/c-TiO$_2$/FA$_x$Cs$_{1-x}$PbI$_3$/Spiro-MeOTAD/Au	1.11	24.88	77.2	21.32	0.09	200 days[c]	2021	47

[a] active area, [b] designated area, c-TiO$_2$: compact TiO$_2$, m-TiO$_2$: mesoporous TiO$_2$. [c] storage stability, [d] operational stability

B. Low vacuum deposition techniques

1. Hybrid chemical vapor deposition method

Chemical vapor deposition is a vacuum-based technique to produce high-quality thin films. In view of operational pressure, modern CVDs can be classified as low-pressure CVD (LPCVD) or ultra-high vacuum CVD (UHVCVD). State-of-the-art CVD prepared perovskite films are deposited at a low vacuum of 10^{-1} - 10^3 Pa, which falls in the LPCVD
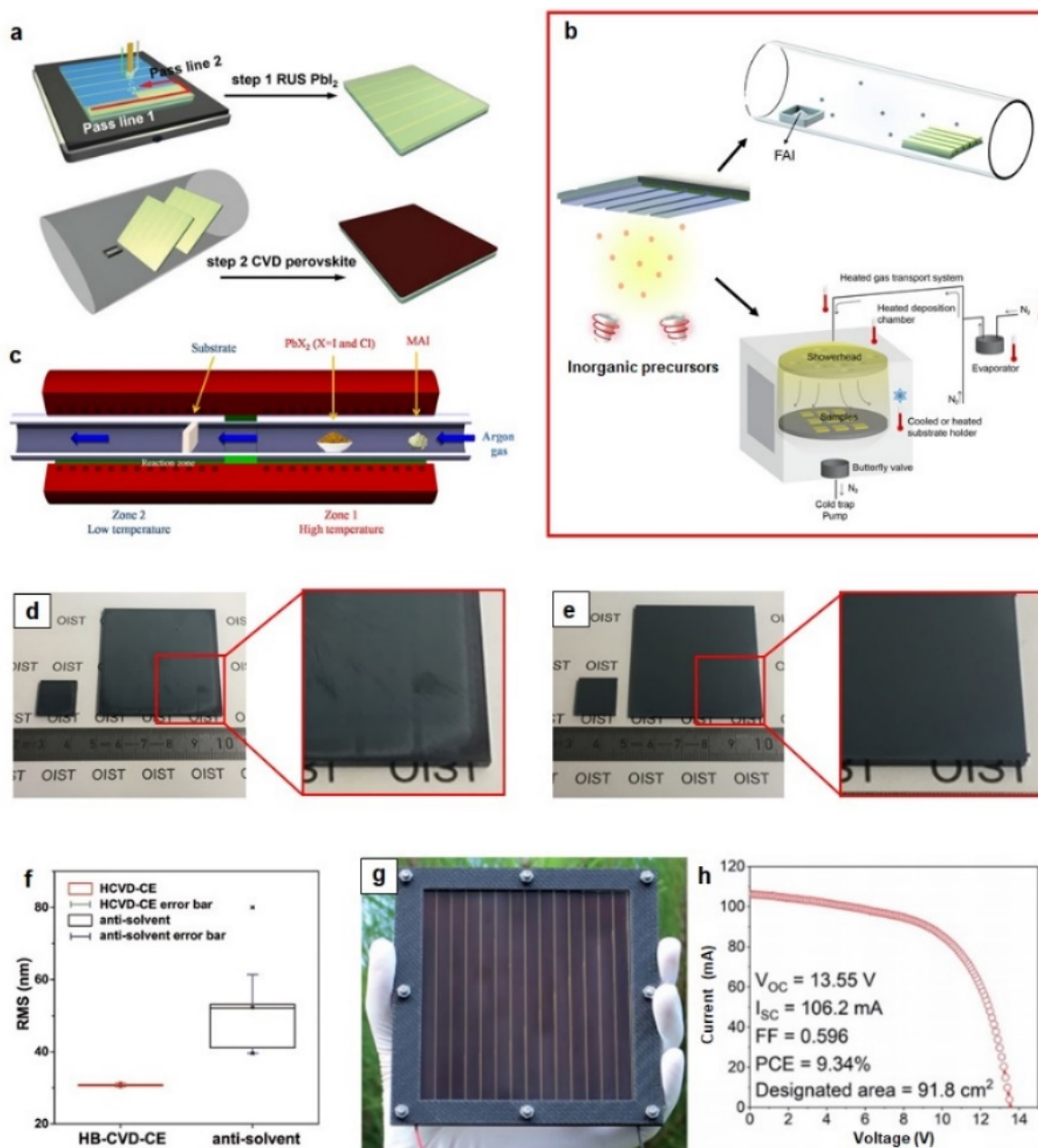
Figure 4. Hybrid chemical vapor deposition of perovskite. Schematic illustration of **(a-b)** hybrid CVD and **(c)** one-step CVD. Photographs of perovskite films prepared by **(d)** two-step spin-coating method and **(e)** HCVD. **(f)** Surface roughness of perovskite films. **(g)** A photograph of a 10 cm × 10 cm sized perovskite mini-module, and **(h)** the J-V characteristics. (a) Reproduced with permission from Adv. Energy Mater. 9, 1803047 (2019). Copyright 2015 Springer Nature. (b) Reproduced with permission from J. Mater. Chem. A 7, 6920 (2019) and ACS Appl. Energy Mater. 4, 4333 (2021). Copyright 2019 Wiley-VCH and copyright 2021 American Chemical Society. (c) Reproduced with permission from J. Solid State Chem. 244, 20 (2016). Copyright 2020 the Royal Society of Chemistry. (d-f) Reproduced with permission from Adv. Funct. Mater. 28, 1703835 (2018). Copyright 2018 Wiley-VCH. (g-h) Reproduced with permission from J. Mater. Chem. A 7, 6920 (2019). Copyright 2019 the Royal Society of Chemistry.

region. A unique advantage of CVD is that highly uniform thin films over an area of m[2] can be obtained, which has been successfully demonstrated in the amorphous Si PV industry.[68] In recent years, CVD has gained increasing attention and becomes an important route among vapor deposition techniques.[72]

In 2014, Qi et al. developed a hybrid CVD (HCVD) approach. Lead halide was deposited on substrates in the first step via scalable methods such as spray coating (**Figure 4a**) or vacuum evaporation (**Figure 4b**), followed by vapor phase deposition of MAI via CVD.[94] Temperatures of the precursor and the substrate zones, vacuum pressure and flow rate of carrier gas are key parameters determining the reaction kinetics. By careful optimization, the authors demonstrated HCVD prepared MAPbI$_3$ PSCs with an efficiency of 11.8% and stability of approximately

1100 h. Later on, Qi et al. showed that the HCVD method can be readily applied for deposition of other perovskites, i.e., $FAPbI_3$,[58, 60, 95] $FA_xCs_{1-x}PbI_3$,[96] $CsPbI_xBr_{3-x}$,[97] with the PCE reaching 16%. Compositions of perovskite determine not only optical absorption but also charge transport characteristics. Perovskite films can also be deposited via a one-step approach by CVD. In 2015, Fan et al. reported a facile one-step CVD to deposit $MAPbI_3$ and $MAPbI_{3-x}Cl_x$ perovskites. Inorganic sources (PbI_2 or $PbCl_2$) and organic sources (i.e., MAI) were loaded in the high-temperature zone, the positions of which were determined by their sublimation temperatures (**Figure 4c**).[98] Meanwhile, the substrates were placed in the low-temperature zone. During the deposition process, a carrier gas (i.e., Ar) was constantly flowed from the source towards the substrate to facilitate the chemical reaction. $MAPbI_3$ and $MAPbI_{3-x}Cl_x$ films with large grains (> 1 μm) and long carrier lifetime were deposited on substrates. The PSCs using these films gave a PCE in the range of 9% to 11%. In 2020, Peng and Ku et al. reported that the incorporation of CsBr significantly improved the crystallinity of the $FAPbI_3$ perovskite. Meanwhile, the FACl vapor could accelerate the perovskite growth rate during the vapor–solid reaction process. Using $Cs_{0.24}FA_{0.76}PbI_{3-y}Br_y$ as the absorber, they obtained a PSC with a PCE of 17.29%[99] and later on 17.77%.[100] In 2021, they developed a multistage atmosphere-assisted (MSA) process. When RbI was introduced in the perovskite system, the halogen exchange can be regulated, allowing passivation of defects in the perovskite layer, especially at the grain boundary. The champion PSC showed a PCE of 19.6%.[101-102]

To demonstrate the processing up-scalability, perovskite layers over a large area (i.e., 5 cm × 5 cm or 10 cm × 10 cm) were prepared by HCVD and compared with those prepared by the spin-coating method. An obvious uniformity improvement was demonstrated by the HCVD processed layer (**Figures 4d** and **e**), which was further confirmed by smaller surface roughness values measured at different positions (**Figure 4f**).[96] These layers were used in the fabrication of perovskite mini-modules. Qi et al. demonstrated Cs-FA mixed cation perovskite solar modules with a PCE of over 14.6% over an active area of 12 cm^2. The mini-module showed only 3.6% relative PCE decay after 3600 h storage in dark, and an average T_{80} lifetime of 388 h under continuous 1-sun equivalent illumination. Recently, Qi et al. discovered that SnO_2 electron transport layer (ETL) deteriorated during the CVD process due to generation of oxygen vacancy defects, and a 5-nm-thick layer of C_{60} deposited on SnO_2 can mitigate such a detrimental effect.[103] Combination of the SnO_2/C_{60} bilayer ETL and HCVD deposited perovskite, Qi et al. fabricated a perovskite mini-module with a PCE approaching 10% over a designated area of 91.8 cm^2 (**Figures 4g** and **h**), and a T_{80} lifetime of approximately 500 h under illumination of 1 sun at 25 °C.[104]

2. Close space sublimation

Close space sublimation (CSS) is another thin-film deposition technique commercially used in the CdTe PVs. In a CSS process, the substrates and source materials are held close to each other (e.g., a few mm) with independent heating elements in a chamber with a low vacuum. The short diffusion path results in a fast thin-film deposition rate (0.5–1.0 μm/min) and a high deposition yield. In 2016, Li et al. used the CSS method to deposit $MAPbI_3$ perovskite.[39] A PbI_2 substrate was pre-deposited and loaded right above the MAI power in a chamber with a low pressure (**Figure 5a**). The temperature of the source was set to be 160 °C for sublimation of MAI and the temperature of the substrate was 150 °C for the subsequent reaction with PbI_2. Lowering the deposition pressure from 50 mbar to 1 mbar facilitated the vapor transport, therefore reducing the processing time from 10 min to 1.5 min (**Figure 5b**). Such a fast conversion rate is highly desirable for roll-to-roll manufacturing. Moreover, the perovskite film showed high uniformity over an area of 5 cm × 5 cm (**Figure 5c**). Using such a CSS deposited perovskite film, an n-i-p structured PSC reached an efficiency of 16.2% (**Figure 5d**). Almost at the same time, Tan et al. reported the application of a CSS deposited p-i-n structured PSC with a similar efficiency.[105] Pérez-Gutiérrez et al. found that the morphology and surface roughness of the perovskite layer could be regulated by tuning the size and crystallinity of PbI_2 grains.[106] Later on, they showed that the halide ratios in the final perovskite film could be easily tuned by adjusting the composition of the organic halide mixtures (i.e., MABr and MACl) for sublimation. By engineering the composition of perovskite, they obtained $MAPb(I_{1-x}Br_x)_3$ and $MAPb(I_{1-x}Cl_x)_3$ PSCs with an efficiency of around 10%.[107] **Table 2** has summarized the PCE and lifetime evolution for the PSCs fabricated by various low vacuum deposition techniques.

III. PROGRESS IN VAPOR DEPOSITION ASSISTED PEROVSKITE SOLAR CELL

The vapor deposition-assisted methods are multi-stage deposition methods that combine the vapor and the solution processes into one. The vapor stage is usually conducted at low vacuum to ambient pressure. Vapor processes such as post deposition treatment (PDT), although are not standalone processes, are considered as the deposition-assisted methods, which are discussed in this section. The vapor deposition-assisted methods take advantage of both the solution-processing (composition and additive engineering, intermediate-phase crystallization kinetics adjustment, defect chemistry regulation, etc.) and the vapor-processing (high uniformity and processing up-scalability, etc.), and may hold the key to fabricating efficient perovskite solar modules. Hereinafter, we introduce several important types of vapor deposition assisted methods.
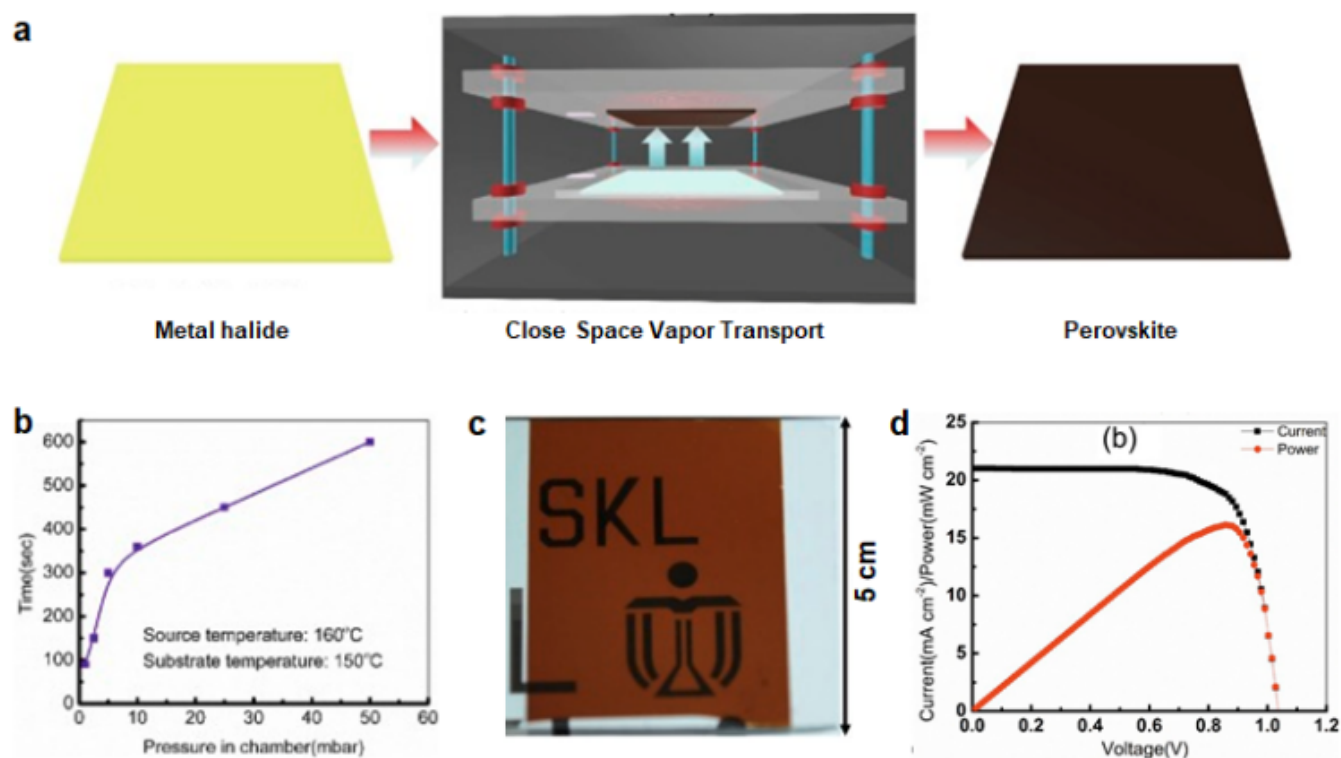
Figure 5. Close space sublimation to deposit perovskite films. (a) Schematic illustration of the CSS method. **(b)** Complete conversion time as a function of deposition pressure. **(c)** A photograph of the CSS deposited $MAPbI_3$ perovskite film. **(d)** I-V and P-V characteristics. (a-d) Reproduced with permission from Status Solidi RRL 10, 153 (2016). Copyright 2016 Wiley-VCH.

TABLE 2. Summary of perovskite solar cells by low vacuum deposition techniques.

Method	Device structure	V_{oc} (V)	Jsc (mA cm^{-2})	FF (%)	η (%)	Area (cm^2)	Lifetime (h)	Year	Reference
Hybrid CVD	FTO/c-TiO$_2$/MAPbI$_{3-x}$Cl$_x$/Spiro-MeOTAD/Au	0.92	19.1	62	10.8	0.07-0.1	1100[c]	2014	94
Hybrid CVD	FTO/c-TiO$_2$/FAPbI$_{3-x}$Cl$_x$/Spiro-MeOTAD/Au	1.03	20.9	66	14.2	0.04-0.16	155 days[c]	2015	95
Hybrid CVD	FTO/c-TiO$_2$/MAPbI$_3$/Spiro-MeOTAD/Ag	0.91	21.7	64.5	12.73	0.12	NA	2015	37
One-step CVD	FTO/c-TiO$_2$/MAPbI$_{3-x}$Cl$_x$/Spiro-MeOTAD/Au	0.97	18	64	11.1	-	NA	2015	98
Hybrid CVD	ITO/ZnPc/MAPbI$_3$/C$_{60}$/Bphen/Al	0.96	17.26	70	11.6	0.032	NA	2016	108
Hybrid CVD	FTO/c-TiO$_2$/MAPbI$_{3-x}$Cl$_x$/Spiro-MeOTAD/Au	1.06	21.7	68	15.6	0.09	NA	2016	58
Hybrid CVD	FTO/c-TiO$_2$/MAPbI$_3$/Spiro-MeOTAD/Au	1.06	22.08	80	18.9	0.11	NA	2016	109
Hybrid CVD	FTO/c-TiO$_2$/FA$_{0.85}$Cs$_{0.15}$PbI$_3$/Spiro-MeOTAD/Ag	0.906	22.858	69.8	14.45	0.12	7 days[c]	2017	110
Hybrid CVD	FTO/c-TiO$_2$/FA$_{0.93}$Cs$_{0.07}$PbI$_3$/Spiro-MeOTAD/Au	1.00	22.0	75.2	16.6	0.09	20[d]	2018	96
Hybrid CVD	FTO/c-TiO$_2$/FA$_{0.93}$Cs$_{0.07}$PbI$_3$/Spiro-MeOTAD/Au	5.84	3.67	68.1	14.6	12[a]	NA	2018	96
Hybrid CVD	FTO/c-TiO$_2$/CsPbBr$_3$/C	1.13	6.79	70	5.38	0.12-0.15	21 days[c]	2018	111
Hybrid CVD	FTO/SnO$_2$/C$_{60}$/FA$_{0.9}$Cs$_{0.1}$PbI$_{2.9}$Br$_{0.1}$/Spiro-MeOTAD/Au	-	-	-	13.3	0.09	500[d]	2019	103
Hybrid CVD	FTO/SnO$_2$/C60/FA$_{0.9}$Cs$_{0.1}$PbI$_{2.9}$Br$_{0.1}$	13.55	1.16	59	9.34	91.8[b]	NA	2019	103

Method	Structure								
	/Spiro-MeOTAD/Au								
Hybrid CVD	FTO/c-TiO$_2$/FAPbI$_x$Br$_{3-x}$/Spiro-MeOTAD/Au	1.03	21.1	74	16.1	2	NA	2019	103
Hybrid CVD	FTO/c-TiO$_2$/FAPbI$_x$Br$_{3-x}$/Spiro-MeOTAD/Au	6.29	3.55	66.5	14.7	12[a]	388[d]	2019	60
Hybrid CVD	FTO/SnO$_2$/C$_{60}$/FA$_{0.9}$Cs$_{0.1}$PbI$_{2.9}$Br$_{0.1}$/Spiro-MeOTAD/Au	0.99	22.3	70.2	15.5	0.09	NA	2020	97
Hybrid CVD	FTO/SnO$_2$/C$_{60}$/FA$_{0.9}$Cs$_{0.1}$PbI$_{2.9}$Br$_{0.1}$/Spiro-MeOTAD/Au	6.8	2.7	67.2	12.3	22.4[b]	NA	2020	97
Hybrid CVD	ITO/PTAA/FA$_x$Cs$_{1-x}$PbI$_3$/PCBM/ZnO/AZO	-	-	-	10.6	0.27	NA	2020	112
Hybrid CVD	ITO/LiF/C$_{60}$/MAPbI$_3$/Spiro-MeOTAD/Au	0.927	17.0	65.4	12.3	0.25	NA	2021	104
Vapor-solid reaction	FTO/SnO$_2$/FA$_x$Cs$_{1-x}$PbI$_{3-y}$Br$_y$/Spiro-MeOTAD/Au	1.065	22.88	71.2	17.29	0.09	200[c]	2018	99
Vapor-solid reaction	FTO/SnO$_2$/FA$_x$Cs$_{1-x}$PbI$_{3-y}$Br$_y$/Spiro-MeOTAD/Au	9.18	2.25	52.8	12.24	41.25[a]	NA	2018	99
Vapor-solid reaction	FTO/SnO$_2$/FA$_x$Cs$_{1-x}$PbI$_{3-y}$Br$_y$/Spiro-MeOTAD/Au	1.02	21.94	78.9	17.66	0.16	60 days[c]	2020	100
Vapor-solid reaction	FTO/SnO$_2$/FA$_x$Cs$_{1-x}$PbI$_{3-y}$Br$_y$/Spiro-MeOTAD/Au	6.28	3.29	67.4	13.92	16.07[b]	NA	2020	100
Vapor-solid reaction	FTO/SnO$_2$/Rb$_{0.04}$-Cs$_{0.14}$FA$_{0.86}$Pb(Br$_y$I$_{1-y}$)$_3$/Spiro-MeOTAD/Au	1.127	22.63	76.8	19.59	0.148	NA	2021	100
Vapor-solid reaction	FTO/SnO$_2$/Rb$_{0.04}$-Cs$_{0.14}$FA$_{0.86}$Pb(Br$_y$I$_{1-y}$)$_3$/Spiro-MeOTAD/Au	6.243	3.51	70	15.35	10[a]	NA	2021	100
Close space sublimation	FTO/c-TiO$_2$/m-TiO$_2$/MAPbI$_x$Cl$_{3-x}$/Spiro-MeOTAD/Au	-	-	-	16.2	0.01	NA	2016	39
Close space sublimation	FTO/PEDOT:PSS/MAPbI$_3$/PCBM/Al	1.03	19.6	80.2	16.2	0.04	NA	2016	105

[a] active area, [b] designated area, c-TiO$_2$: compact TiO$_2$, m-TiO$_2$: mesoporous TiO$_2$. [c] storage stability, [d] operational stability

A. Vapor-assisted solution process

Vapor-assisted solution process (VASP) is one of the first vapor deposition assisted methods developed by Yang et al. to fabricate organic/inorganic hybrid perovskite films (e.g., MAPbX$_3$, X = Cl, Br, I) in 2014.[113] The PbI$_2$ framework films were prepared by spin-coating, followed by the treatment with an organic vapor (i.e., MAI) (**Figure 6a**). This method takes advantage of the kinetic reactivity of MAI and thermodynamic stability of perovskite and results in polycrystalline perovskite thin films with full surface coverage (**Figure 6b** inset), low surface roughness, and large grain size. Solar cells with a planar structure achieved a PCE of 12.1% (**Figure 6b**). In 2015, Sharp et al. developed a low-pressure VASP method, where the reaction between PbI$_2$/PbCl$_2$ mixture films and the MAI vapor is conducted at 0.3 Torr (**Figure 6c**).[49] Low pressure enables the annealing temperature (120 °C) to be reduced with respect to ambient pressure VASP (150 °C). The LP-VASP processed perovskite film, when constructed in a planar structured PSC, resulted in a champion PCE of 16.8% with reduced J-V hysteresis (**Figure 6d**). They indicated that the effect of Cl on carrier lifetime in LP-VASP processed perovskite was less significant compared to the solution-processed perovskite solar cells. This is likely due to the halide exchange between Cl$^-$ and I$^-$ during the LP-VASP process. Yao et al. showed that by varying the ratio between the MAI and FAI mixture powder during LP-VASP, a series of mixed cation perovskites (i.e., FA$_x$MA$_{1-x}$PbI$_3$) can be easily prepared. The PSCs using FA$_{0.6}$MA$_{0.4}$PbI$_3$ as absorbers achieved a champion PCE of 16.48%.[114]

B. Hybrid vapor-solution process

The hybrid vapor-solution process is conceptually similar to VASP, but the vapor and solution processing is conducted in a reverse sequence. In short, the inorganic templates are vapor-deposited, followed by perovskite conversion via a solution process (**Figure 7a**). This method shows a unique advantage towards deposition of uniform perovskite layers on substrates with textures or large surface roughness. Rafizadeh et al. systematically studied the concentration of MAI on the perovskite crystallization and grain growth. At a low MAI concentration, conversion of perovskite is incomplete, resulting in substantial unreacted PbI$_2$ and formation of voids in the as-prepared film. While at a high MAI concentration, the grain growth
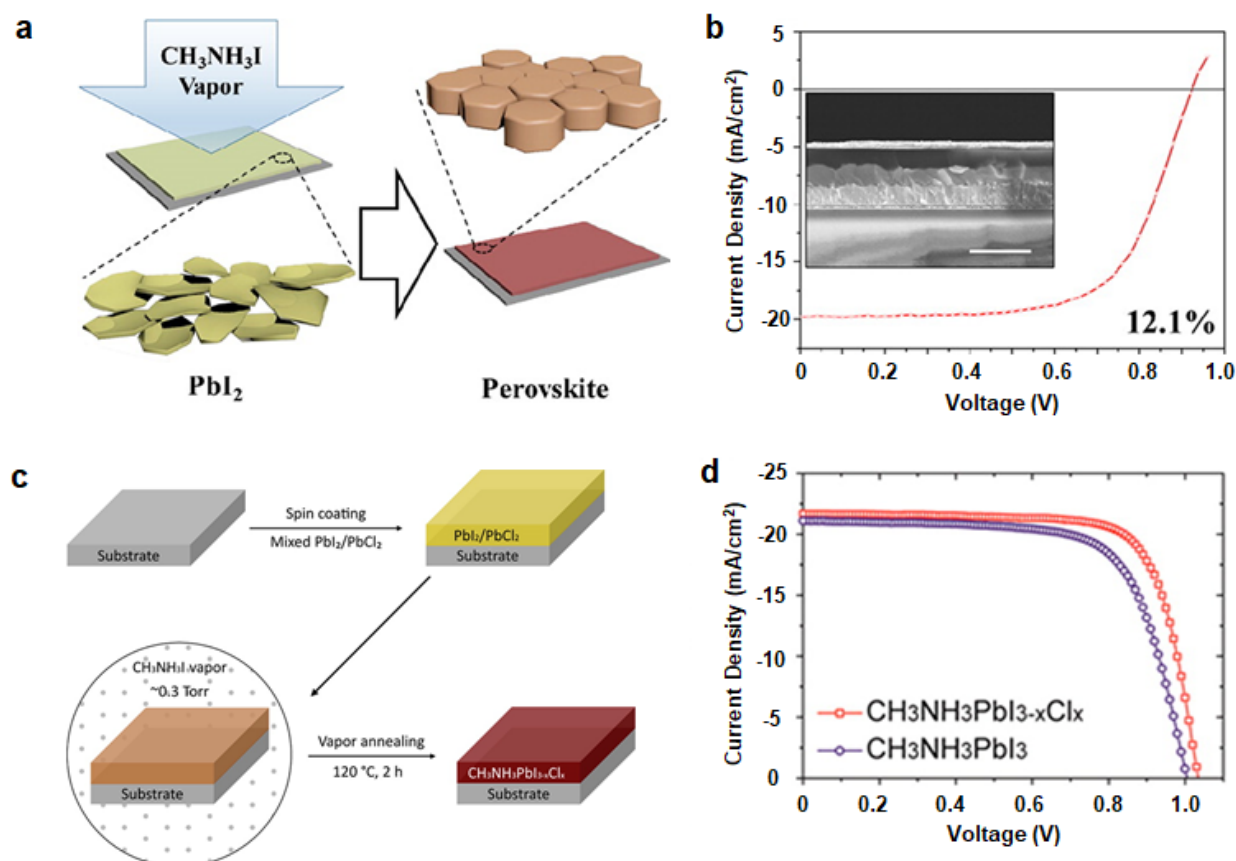
Figure 6. Vapor-assisted solution process. (a) Schematic illustration of VASP. **(b)** J-V curve of the PSC fabricated by VASP. Inset is the cross-section image of the PSC with a scale bar of 1 μm. **(c)** Schematic illustration of the LP-VASP and **(d)** the J-V curves of PSCs fabricated by VASP. (a-b) Reproduced with permission from J. Am. Chem. Soc. 136, 622 (2013). Copyright 2014 American Chemical Society. (c-d) Reproduced with permission J. Phys. Chem. Lett. 6, 493 (2015). Copyright 2015 American Chemical Society.

causes the appearance of gaps between the adjacent grains. With a suitable MAI concentration, the PSC reached a PCE of 18.2% with small hysteresis.[115] Bolink et al. advanced this technique for preparation of mixed halide perovskite. By optimizing the deposition rate of the PbI_2 layer and by inserting small amounts of MABr and MACl to the MAI salt in the solution-based conversion step, they obtained a PSC ($ITO/MoO_x/TaTm/MAPbI_{3-x-y}Br_xCl_y/C_{60}/BCP/Ag$) with low dark current and a PCE of 19.8% (**Figures 7b** and **c**).[116]

In tandem applications, PSCs are used as the top cells, which are to be deposited on the bottom cells with textures (i.e., silicon) or high surface roughness (i.e., CIGS).[117] Conventional solution methods could not produce conformal layers on such textured substrates, resulting in severe shunting losses.[118-120] In 2018, Yang et al. developed a chemical mechanical polishing method to create a smooth interconnecting layer (i.e., ITO) in perovskite/CIGS two-terminal tandem devices. This approach allows the adoption of solution processing of perovskite on top of the CIGS bottom cell but at the cost of optical loss.[121] In 2018, Jeangros et al. reported using the hybrid vapor-solution method to deposit perovskite films on textured silicon substrates for tandem applications. The growth of a perovskite layer followed well the texture of silicon pyramids (**Figures 7d** and **e**). As a result, they fabricated monolithic perovskite/silicon tandem solar cells with a PCE of 25.2%.[122]

C.   MA gas assisted perovskite formation

In 2015, Pang and Cui et al. discovered that the $MAPbI_3$ perovskite crystals could be "melted" in the presence of CH_3NH_2 gas within a few minutes.[123] Further exposure in CH_3NH_2 gas atmosphere led to the transformation from a black solid crystal to a transparent liquid phase according to Equation 1.

$$CH_3NH_3PbI_3(s) + xCH_3NH_2(g) \rightarrow CH_3NH_3PbI_3 \bullet xCH_3NH_2(l)$$
(1)
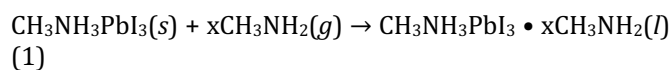
Removing the CH_3NH_2 gas resulted in recrystallization of perovskite via CH_3NH_2 outgassing, as described in Equation 2 and indicated by the color change from transparent to black (**Figure 8a**).
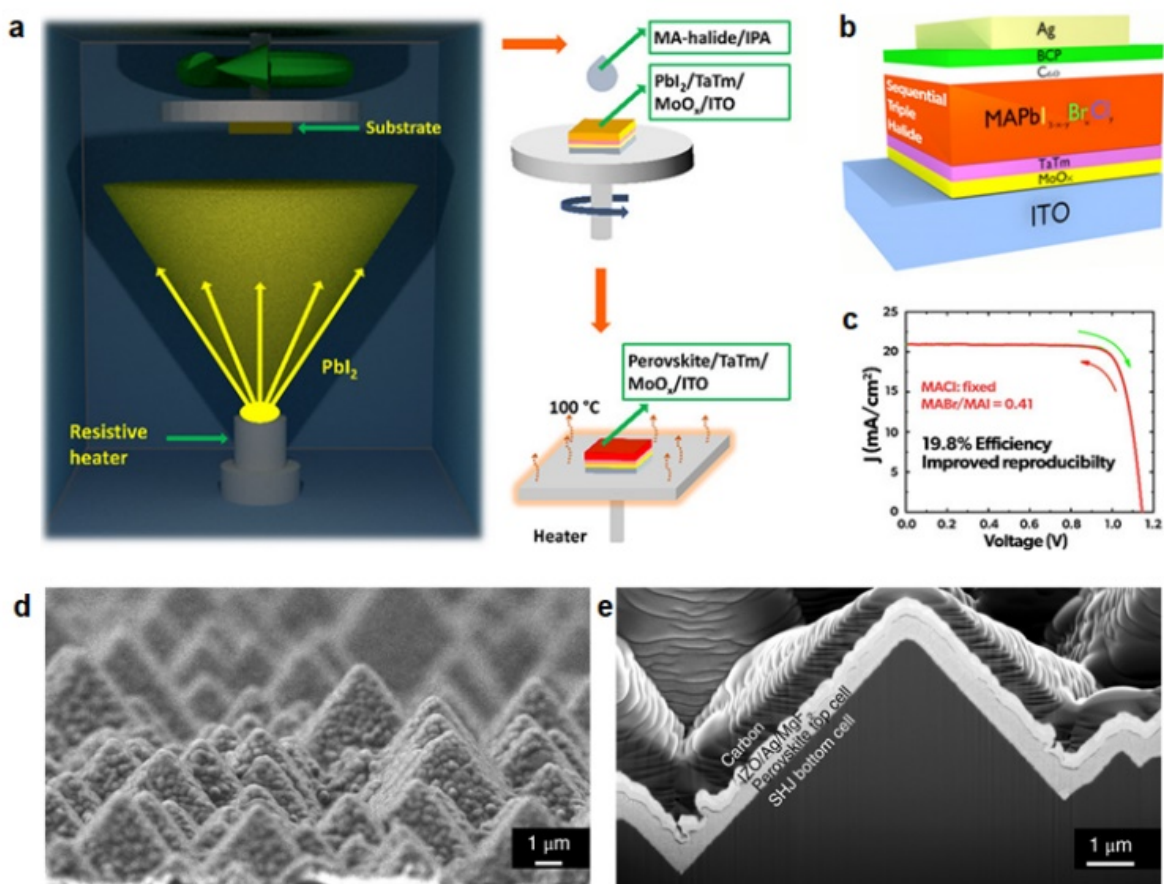
Figure 7. Hybrid vapor-solution process. (a) Schematic illustration of the hybrid vapor-solution process. **(b)** Structure and **(c)** J-V curves of the PSC. **(d)** Top view and **(e)** cross-section SEM images of the perovskite top cell deposited on textured silicon heterojunction bottom cell. (a-c) Reproduced with permission from ACS Appl. Energy Mater. 3, 8257 (2020). Copyright 2020 American Chemical Society. (d-e) Reproduced with permission from Nat. Mater. 17, 820 (2018). Copyright 2018 Springer Nature.

$$CH_3NH_3PbI_3 \bullet xCH_3NH_2(l) \rightarrow CH_3NH_3PbI_3(s) + xCH_3NH_2(g) \quad (2)$$
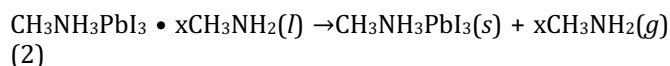
This unique feature allowed healing defects in polycrystalline perovskite films, resulting in mirror-like films with preferred crystalline orientation (**Figure 8b**) and enhanced electronic quality. Later on, Pang et al., showed that a similar solid-liquid-solid phase transition occurs when exposing methylamine to NH_4PbI_3,[124] $HPbI_3$[125] and CsI.[126] Therefore, a series of methylamine-induced conversion processes were demonstrated. In 2016, Qi et al. reported a rapid perovskite formation method when pre-deposited PbI_2 films were sequentially exposed to CH_3NH_2 and HI gases. The perovskite films were obtained within a few seconds of exposure and exhibited complete coverage with a surface roughness of 2 nm.[127] Later on, they developed a methylamine post-annealing treatment for $MAPbI_3$ perovskite.[25, 128] The spin-coated wet perovskite precursor films were annealed in the CH_3NH_2 atmosphere instead of the conventional thermal annealing (**Figure 8c**). The process promoted

continuity between adjacent grains (**Figures 8d** and **e**) and greatly reduced metallic Pb impurities at perovskite grain boundaries (**Figure 8f**). As a result, the PSCs achieved a PCE of up to 18.4% with significantly improved stability.

The CH_3NH_2 gas-induced perovskite formation process demonstrates a great potential for large-area manufacturing. In 2017, Chen et al. developed a solvent and vacuum-free route for fabrication of perovskite solar modules. They showed that a transparent liquid phase of the amine complex, $CH_3NH_3I \cdot mCH_3NH_2$ (m = 3) was formed by the interaction between CH_3NH_3I and CH_3NH_2 molecules (Equation 3).

$$CH_3NH_3I(s) + mCH_3NH_2(g) \leftrightarrow CH_3NH_3I \bullet mCH_3NH_2(l) \quad (3)$$
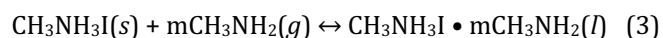
The amine complex precursors, $CH_3NH_3I \cdot 3CH_3NH_2$ and $PbI_2 \cdot CH_3NH_2$, were mixed and the perovskite films were fabricated by a pressure processing method. The deposited perovskite films were highly uniform without pinholes. Using such a method, a perovskite mini-module with a certified PCE of 12.1% over an aperture area
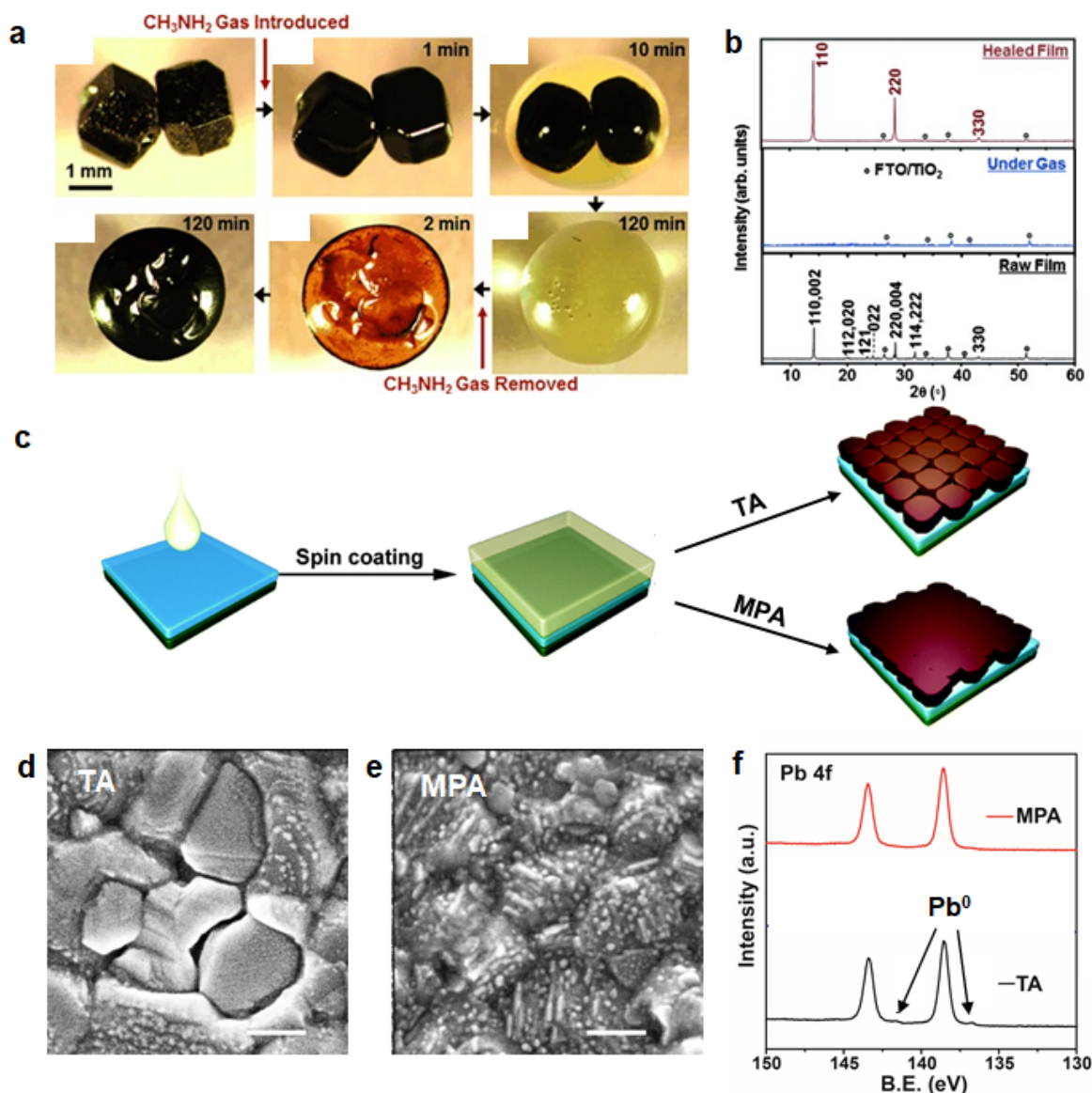
Figure 8. MA gas-assisted perovskite formation. **(a)** Optical images showing the methylamine-induced solid-liquid-solid evolution. **(b)** XRD patterns of the polycrystalline perovskite films. **(c)** Schematic illustration of the methylamine post-annealing process. TA and MPA are thermal annealing and methylamine post-annealing. SEM images of the perovskite films by **(d)** TA and **(e)** MPA. **(f)** XPS spectra of the TA and MPA prepared perovskite films. (a-b) Reproduced with permission from Angew. Chem. Int. Ed. 54, 9705 (2015). Copyright 2015 Wiley-VCH. (c-f) Reproduced with permission from Mater. Horiz. 3, 548 (2016). Copyright 2018 the Royal Society of Chemistry.

of 36.1 cm^2 was realized.[55]Qi et al. incorporated the chlorine in HPbI$_3$(Cl) before exposing it to the CH$_3$NH$_2$ gas, which allowed fabrication of 1-μm-thick perovskite films with high crystallinity, low defect density and long carrier lifetime. A 12.0 cm^2 six-cell perovskite solar module with a PCE of 15.3% was demonstrated.[50]

D. MASCN gas assisted perovskite formation

FAPbI$_3$ is an ideal absorber candidate because of the proper bandgap and high thermal stability compared to MAPbI$_3$. However, the thermodynamically stable δ-phase of FAPbI$_3$ at solar cell operational temperature is photo-inactive. It is necessary to find methods to stabilize FAPbI$_3$ in the photoactive α-phase.[129] In 2020, Grätzel et al. reported that the treatment of the δ-phase FAPbI$_3$ films with MASCN vapor caused the phase transition temperature from the δ to α phase to reduce below 150 °C.[51] Upon MASCN vapor exposure, I$^-$ ions bonded to Pb^{2+} on the surface of δ-FAPbI$_3$ were substituted by SCN$^-$ ions, which disintegrated the top layer of face-sharing octahedra and induced the transition to the corner-sharing architecture of α-FAPbI$_3$.

Solid-state nuclear magnetic resonance (ssNMR) and time-of-flight secondary ion mass spectrometry (Tof-SIMS)

measurements indicated that MASCN was not incorporated into the perovskite lattices but rather interacted with the $FAPbI_3$ surface. Such a $FAPbI_3$ film was maintained in the α phase after annealing at 85 °C for 500 h, whereas the reference film decomposed to PbI_2 severely. In addition, the MASCN vapor-treated film showed stronger absorption and photoluminescent (PL) intensity. Using the MASCN gas assisted perovskite formation method, PSCs with a structure of $ITO/SnO_2/FAPbI_3/Spiro$-MeOTAD/Au were prepared, showing a champion PCE of over 23%. Furthermore, the device exhibited a high external quantum efficiency of electroluminescent (EL) (6.5% with an injection current density of 25 mA/cm^2) and a record low turn-on voltage (i.e., 0.75V). **Table 3** has summarized the PCE and lifetime evolution for the PSCs fabricated by various vapor deposition-assisted techniques.

TABLE 3. Summary of vapor deposition-assisted perovskite solar cells.

Method	Device structure	V_{oc} (V)	Jsc (mA cm^{-2})	FF (%)	η (%)	Area (cm^2)	Lifetime (h)	Year	Reference
Vapor-assisted solution process (VASP)	FTO/c-$TiO_2/MAPbI_3/Spiro$-MeOTAD/Ag	0.924	19.8	66.3	12.1	0.12	NA	2013	113
VASP	FTO/c-$TiO_2/MAPbI_{3-x}Cl_x/Spiro$-MeOTAD/Au	1.04	21.7	75	16.8	0.062	NA	2015	49
VASP	FTO/c-$TiO_2/C60/FA_xMA_{1-x}PbI_3/Spiro$-MeOTAD/Au	1.00	22.51	76.56	16.48	0.09	NA	2017	114
MASCN treatment	$ITO/SnO_2/FAPbI_3/Spiro$-MeOTAD/Au	1.165	24.4	81.3	23.1	0.16	500[d]	2020	51
CH_3NH_2 treatment	FTO/c-TiO_2/m-$TiO_2/MAPbI_3/Spiro$-MeOTAD/Ag	1.08	19.6	71.4	15.1	0.09	NA	2015	123
CH_3NH_2 treatment	FTO/c-TiO_2/m-$TiO_2/MAPbI_3/Spiro$-MeOTAD/Ag	1.03	21.5	77.9	17.3	0.09	NA	2016	124
CH_3NH_2 treatment	FTO/c-TiO_2/m-$TiO_2/MAPbI_3/Spiro$-MeOTAD/Ag	1.04	21.8	80	18.2	0.09	NA	2016	125
CH_3NH_2 treatment	FTO/c-TiO_2/m-$TiO_2/MAPbI_3/Spiro$-MeOTAD/Au	1.11	21.6	77	18.4	0.09	8 days[c]; 2[d]	2016	25
CH_3NH_2 treatment	FTO/c-TiO_2/m-$TiO_2/MAPbI_3/Spiro$-MeOTAD/Au	1.04	21.8	72	16.32	-	NA	2016	130
CH_3NH_2 treatment	FTO/c-TiO_2/m-$TiO_2/MA_{0.9}Cs_{0.1}PbI_3/Spiro$-MeOTAD/Au	1.10	20.97	74.04	17.08	0.09	NA	2017	126
CH_3NH_2 treatment	FTO/c-TiO_2/m-$TiO_2/MAPbI_3/Spiro$-MeOTAD/Au	1.12	22.6	76.2	19.3	1.0	500[d]	2017	55
CH_3NH_2 treatment	FTO/c-TiO_2/m-$TiO_2/MAPbI_3(Cl)/Spiro$-MeOTAD/Au	1.11	22.9	79.1	20.0	0.09	1600[d]	2018	50
CH_3NH_2 treatment	FTO/c-TiO_2/m-$TiO_2/MAPbI_3(Cl)/Spiro$-MeOTAD/Au	6.65	3.66	63	15.3	12.0[a]	NA	2018	50
CH_3NH_2 treatment	FTO/c-TiO_2/m-$TiO_2/MAPbI_3/Spiro$-MeOTAD/Au	1.178	22.81	79.5	21.36	0.0725	1000[d]	2020	131
MA+HI treatment	FTO/c-TiO_2/m-$TiO_2/MAPbI_3/Spiro$-MeOTAD/Au	1.05	20.6	71	15.3	0.05-0.18	133 days[c]	2016	127
MA+HI treatment	FTO/c-TiO_2/m-$TiO_2/MAPbI_3/Spiro$-MeOTAD/Au	1.04	18.6	67	12.9	-	NA	2020	132
Vapor-Solution sequential deposition	FTO/c-$TiO_2/PCBM/MAPbI_3/Spiro$-MeOTAD/Au	1.103	22.95	74.5	18.9	0.16	NA	2019	115
Vapor-Solution sequential deposition	$ITO/MoO_x/TaTm/MAPbI_{3-x-y}Br_xCl_y/C_{60}/BCP/Ag$	1.15	21.2	81.7	19.8	0.06	90[d]	2020	116

[a] active area, [b] designated area, c-TiO_2: compact TiO_2, m-TiO_2: mesoporous TiO_2. [c] storage stability, [d] operational stability
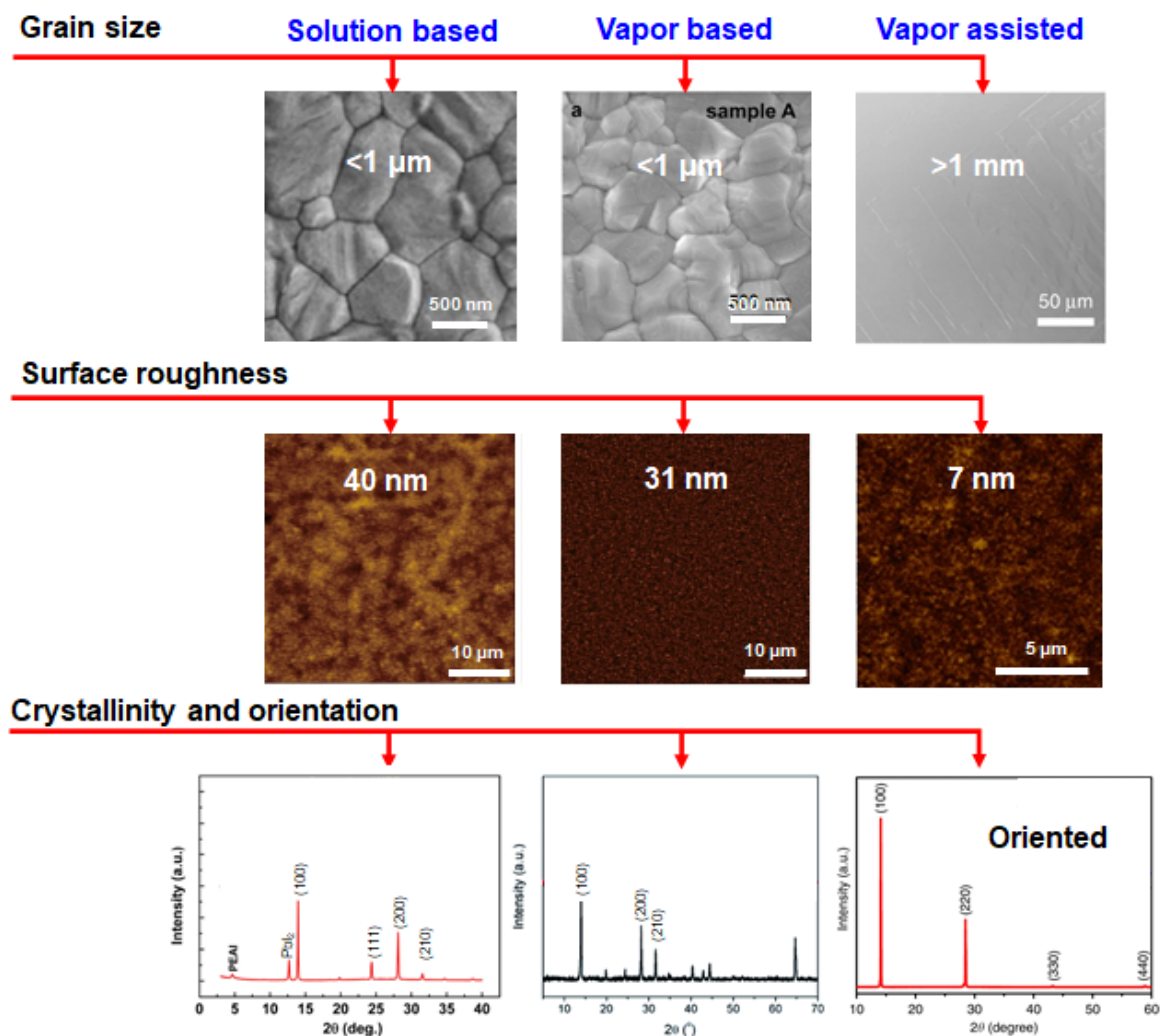
Figure 9. Morphology, surface roughness, crystallinity and crystallographic orientation of perovskite films prepared by different methods. The data are collected from published papers.[44, 96-97, 131, 133] Reproduced with permission from Nat. Photonics 13, 460 (2019), Adv. Funct. Mater. 28, 1703835 (2018), J. Mater. Chem. A 8, 23404 (2020), Nat. Commun. 11, 5402 (2020), Nature 590, 587 (2021). Copyright 2019, 2020, 2021 Springer Nature; Copyright 2018 Wiley-VCH; Copyright 2020 the Royal Society of Chemistry.

IV. COMPARISONS BETWEEN VAPOR AND SOLUTION-PROCESSED PEROVSKITE

Based on this review in vapor deposition-based and assisted perovskites, one can conclude that the deposition processes of VDBA are quite different from solution processes in view of equipment to use (chambers or tubes connecting to vacuum systems, in-situ film thickness monitoring system, mass flow control systems, etc.) and key parameters to control (deposition pressure (i.e., background pressure), partial pressure of source vapor, flow of carrier gas, temperature of the substrate, to name a few). The different deposition processes result in perovskite films that are different in morphology, crystallinity and crystallographic orientation. To give a clear overview, we selected perovskite films prepared by solution-based method, vapor-based method and vapor-assisted method, respectively, and compared these important characteristics (**Figure 9**). Samples are selected according to the following criteria. (I) They are either standard samples representing common features of perovskite films deposited by such methods (i.e., solution-based and vapor-based method) or the sample that gives the best feature (i.e., vapor-assisted method). (II) These perovskite films, when constructed in a solar cell, give state-of-the-art PCE. From the morphology viewpoint, perovskite films prepared by solution and vapor-based methods both show a polycrystalline nature with a typical grain size of less than 1 μm. In strict contrast, perovskite film prepared by vapor assisted methods (e.g., MA gas assisted method) shows a single-crystal characteristic with grain size over 1 mm (**Figure 9**). Besides, solution and vapor-based methods deposited perovskite films have
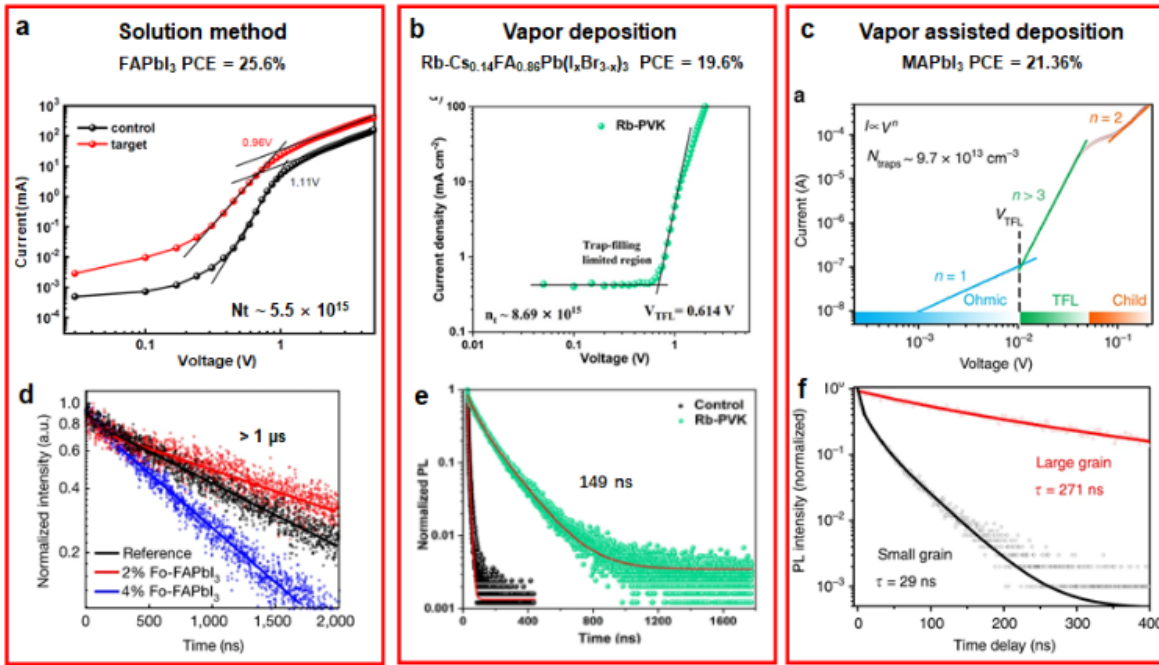
Figures 10. Defect density and carrier lifetime of perovskites prepared by different methods. (a, d) Solution-based method, **(b, e)** vapor deposition based method and **(c, f)** vapor deposition assisted method. (a, d) Reproduced with permission from Nature 592, 381 (2021). Copyright 2021 Springer Nature. (b, e) Reproduced with permission from Sustain. Energy Fuels 4, 2491 (2020). Copyright 2021 Wiley-VCH. (c, f) Reproduced with permission from Chem. Mater. 28, 284 (2015). Copyright 2020 Springer Nature.

surface roughness on tens of nm scale. It is worth mentioning that some vapor processed perovskite films (i.e., co-evaporation) have a low surface roughness of a few nanometers. Whereas the vapor-assisted method processed film has a small surface roughness value. From the crystallinity's viewpoint, solution and vapor-based methods deposited perovskite films exhibits moderate crystallinity. On the other hand, the vapor-assisted method deposited perovskite exhibits a higher degree of crystallinity, agreeing well with the grain feature. Furthermore, the vapor-assisted method deposited perovskite shows a preferred crystallographic orientation as compared to the other two methods.

The morphology and crystallinity qualities determine the density of defects and charge transport kinetics in the polycrystalline perovskite films. The space-charge limited current (SCLC) method is usually applied to quantitatively calculate the trap density in perovskite films (**Figures 10a-c**).[134-135] The dark current-voltage (I–V) measurements are conducted on the devices and the trap densities (N_t) are calculated using Equation 4,

$$N_t = 2\varepsilon\varepsilon_0 V_{TFL}/eL^2 \qquad (4)$$

where ε_0 is the vacuum permittivity, ε is the relative dielectric constant of perovskite, e is the electron charge, and L is the thickness of the perovskite film. When the comparison is made between perovskite films prepared

by the different methods, a trend can be concluded as follows. The trap densities in solution and vapor-based methods deposited perovskite films are similar (i.e., 10^{15} cm^{-3}),[45, 102] which are 1 order of magnitude higher than the vapor assisted method deposited perovskite (i.e., 10^{14} cm^{-3}).[131] Generally speaking, these traps are responsible for carrier trapping and non-radiative recombination, causing electrical losses in PSCs. However, it is interesting to note that defect densities in vapor based and assisted methods prepared perovskites films are similar or lower than those prepared by solution methods. This observation suggests that density of defects may not be the key limitation in vapor based and assisted methods prepared perovskites.

Among various techniques (transient absorption, time-resolved THz spectroscopy, time-resolved microwave conductivity) to study charge transport kinetics of perovskite absorbers,[136] time-resolved photoluminescence (TRPL) measurement is the most commonly used technique (**Figures 10d-f**). Carrier lifetime (τ), defined as the average time it takes for minority carriers to recombine, can be obtained from perovskite layers that are deposited by different methods. Solution-processed perovskites show a typical carrier lifetime of over 1 μs.[45] As a comparison, vapor-based and assisted methods prepared perovskites show carrier lifetimes that are one magnitude lower.[102, 131] A longer carrier lifetime resulted in a longer carrier diffuse length, L (Equation 5).
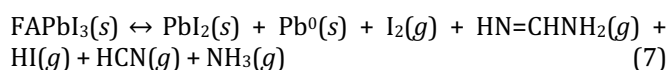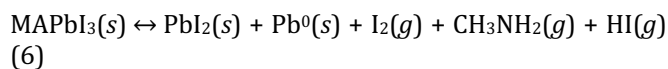
$$L = \sqrt{D\tau} \qquad (5)$$

where D is diffusion coefficient (diffusivity). Considering that the thickness of perovskite absorbers should be smaller than L to allow photo-generated carriers to be collected before recombination, a larger τ value is a benefit for efficient carrier transport (assuming that D is constant). Record PCEs of perovskite solar cells prepared by different methods followed the trend of perovskite carrier lifetime, indicating that carrier lifetime could be a limiting factor. Therefore, strategies towards improving the carrier lifetime of perovskite absorbers could be a rational approach to enhance the PCE of vapor-based and assisted perovskite solar cells.

V. SUMMARY AND OUTLOOK

The applications of vapor deposition based and assisted methods in fabrication of polycrystalline perovskite films are gaining increasing attention due to the superior advantages such as fewer solvent concerns, high uniformity over large-area and the possibility to integrate with existing thin-film PV manufacturing lines. Although research efforts have been made to advance the VDBA method and significant achievements are obtained in terms of perovskite electronic quality, one can see that efficiencies of the state-of-the-art VDBA processed PSCs are far from the theoretical limit. Meanwhile, other important criteria such as stability and cost-performance analyses should be considered when the technology roadmap is to be planned. In the following section, we provide hints on several future research directions regarding the VDBA method.

A. Formation and decomposition kinetics of vapor-deposited perovskite

Perovskites are known to be a class of structurally soft materials. In a vapor deposition-based process, the growth of perovskite is conducted at a high temperature and in a vacuum environment with a constant supply of organic halide vapor. Meanwhile, thermal annealing and vacuum conditions can trigger the decomposition of perovskite, accompanied by outgassing of organic components such as CH_3NH_2, HI, CH_3I, NH_3, and I_2 from the $MAPbI_3$ (Equation 6) and $HN=CHNH_2$, HI, HCN, and NH_3 from $FAPbI_3$ (Equation 7), respectively.[137-138]

$$MAPbI_3(s) \leftrightarrow PbI_2(s) + Pb^0(s) + I_2(g) + CH_3NH_2(g) + HI(g) \quad (6)$$

$$FAPbI_3(s) \leftrightarrow PbI_2(s) + Pb^0(s) + I_2(g) + HN=CHNH_2(g) + HI(g) + HCN(g) + NH_3(g) \quad (7)$$

When the forward reaction proceeds at the same rate as the reverse reaction, a chemical equilibrium is created. Growth of perovskite is a dynamic process that is determined by the formation and decomposition kinetics. A fundamental understanding of formation and decomposition kinetics of the vapor deposition processes may be an important task to fabricate high-quality

perovskite films with negligible decomposition byproducts.

B. Defect chemistry in vapor deposition based and assisted perovskite

Structural defects and impurities in perovskite semiconductors play a vital role in solar cell performance. State-of-the-art understanding of defect chemistry in perovskites explains well the case of solution-processed perovskites.[15] Many defect passivation strategies (alkali metal halide treatments,[139] 2D/3D perovskite formation,[140] interface passivation[141]) have been developed, which can mitigate the electrical losses and boost the PCE of the solution-processed PSCs. These strategies, however, may not work for vapor deposition based and assisted perovskite. A possible explanation is that solution and vapor processed perovskites experience different nucleation and grain growth process. The detrimental defects that dominate the electronic quality of polycrystalline films are different. From this viewpoint, an understanding of defect chemistry in vapor deposition based and assisted perovskite (i.e., defect types, densities, locations and energy levels) is needed, which may shed light on the development of advanced defect passivation strategies to further boost solar cell efficiency.

C. Processing throughput of the VDBA processed perovskite solar cells

Processing throughput is a key parameter that determines the manufacturing cost of perovskite solar cells. Song et al. reported that increasing the throughput from 0.53 m^2 min^{-1} to 1.44 m^2 min^{-1} (close to real thin-film PV manufacturing scenario) reduced the manufacturing cost by ~20%.[142] Among the VDBA methods, close space sublimation is a fast deposition technique commercially used in the CdTe PV industry.[71] The conversion of perovskite using the CSS method can be realized in a few minutes without any post-annealing treatment. On the other hand, deposition of the inorganic framework (i.e., thermal evaporation) consumes a longer time and becomes the bottleneck of the process. From this viewpoint, high-throughput methods for deposition of the inorganic framework should be developed.

D. Stability of the VDBA processed PSCs

Several reports have indicated that perovskite deposited by VDBA methods exhibited higher stability compared with solution methods.[78] When using the VDBA processed perovskite layers in PSCs, operational stability (i.e., under 1-sun illumination) varies significantly from a few hours up to 1600 h (Table 1, 2). The relatively large variation in solar cell lifetime makes it difficult to compare between different deposition methods. Moreover, most of the stability measurements for the VDBA processed PSCs were shelf lifetime measurements, which could not reflect the device lifetime under realistic operation conditions. A consensus statement for the stability assessment of PSCs

has been reported in 2020.[143] A series of testing protocols were recommended, including light-soaking (ISOS-L), bias stability (ISOS-V), outdoor stability (ISOS-O), thermal cycling (ISOS-T) and light cycling (ISOS-LC). Following these testing protocols to study the lifetime of VDBA processed PSCs could facilitate the community to compare the results obtained from different institutes. A deep understanding of degradation mechanisms in VDBA processed PSCs can be gained.

E. Roll-to-roll manufacturing perovskite films with a size of m²

A unique advantage of the vapor deposition method is to deposit uniform thin films over an area of m² as demonstrated in the amorphous Si PV industry. The VDBA methods such as hybrid CVD have shown a great potential to deposit perovskite films over a similar scale. A proof-of-concept perovskite solar module demonstration with a size of m² scale would be the next giant leap toward technology commercialization. The facilities and infrastructures that are compatible with roll-to-roll manufacturing could be investigated. The power output of perovskite solar modules operated in outdoor conditions should be tested.

AUTHOR DECLARATIONS CONFLICT OF INTEREST

The authors declare no conflict of interest.

DATA AVAILABILITY STATEMENT

The data that support the findings of this study are available from the corresponding author upon reasonable request.

REFERENCES

[1] 12.4 TW of solar PV by 2050 forecast (PVTECH, accessed: 2021). https://www.pv-tech.org/analysis-20-fold-growth-and-12-4tw-by-2050-forecast-but-solar-pv-could-still-do-more/.

[2] T. Wu, Z. Qin, Y. Wang, Y. Wu, W. Chen, S. Zhang, M. Cai, S. Dai, J. Zhang, J. Liu, Z. Zhou, X. Liu, H. Segawa, H. Tan, Q. Tang, J. Fang, Y. Li, L. Ding, Z. Ning, Y. B. Qi, Y. Zhang and L. Han, Nano-Micro Lett. **13**, 152 (2021).

[3] A. Kojima, K. Teshima, Y. Shirai and T. Miyasaka, J. Am. Chem. Soc. **131**, 6050-6051 (2009).

[4] M. A. Green, A. Ho-Baillie and H. J. Snaith, Nat. Photonics **8**, 506-514 (2014).

[5] N.-G. Park, Mater. Today **18**, 65-72 (2015).

[6] M. M. Lee, J. Teuscher, T. Miyasaka, T. N. Murakami, H. J. Snaith, Science **338**, 643-647 (2012).

[7] M. Liu, M. B. Johnston and H. J. Snaith, Nature **501**, 395-398 (2013).

[8] Z. Hu, Z. Lin, J. Su, J. Zhang, J. Chang and Y. Hao, Solar RRL **3**, 1900304 (2019).

[9] D. W. d. Quilettes, S. M. Vorpahl, S. D. Stranks, H. Nagaoka, G. E. Eperon, M. E. Ziffer, H. J. Snaith and D. S. Ginger, Science **348**, 683-686 (2015).

[10] S. D. Stranks, G. E. Eperon, G. Grancini, C. Menelaou, M. J. Alcocer, T. Leijtens, L. M. Herz, A. Petrozza and H. J. Snaith, Science **342**, 341-344 (2013).

[11] C. Wehrenfennig, G. E. Eperon, M. B. Johnston, H. J. Snaith and L. M. Herz, Adv. Mater. **26**, 1584-1589 (2014).

[12] G. Xing, N. Mathews, S. Sun, S. S. Lim, Y. M. Lam, M. Grätzel, S. Mhaisalkar and T. C. Sum, Science **342**, 344-347 (2013).

[13] W.-J. Yin, T. Shi and Y. Yan, A. Phys. Lett. **104**, 063903 (2014).

[14] W. J. Yin, T. Shi and Y. Yan, Adv. Mater. **26**, 4653-4658 (2014).

[15] L. K. Ono, S. F. Liu and Y. B. Qi, Angew. Chem. Int. Ed. **59**, 6676-6698 (2020).

[16] R. E. Brandt, J. R. Poindexter, P. Gorai, R. C. Kurchin, R. L. Z. Hoye, L. Nienhaus, M. W. B. Wilson, J. A. Polizzotti, R. Sereika, R. Žaltauskas, L. C. Lee, J. L. MacManus-Drisco, M. Bawend, V. Stevanović and T. Buonassisi, Chem. Mater. **29**, 4667-4674 (2017).

[17] Best Research-Cell Efficiency Chart (NREL, accessed: 2021). https://www.nrel.gov/pv/cell-efficiency.html.

[18] G. Grancini, C. Roldán-Carmona, I. Zimmermann, E. Mosconi, X. Lee, D. Martineau, S. Narbey, F. Oswald, F. D. Angelis, M. Graetzel and M. K. Nazeeruddin, Nat. Commun. **8**, 15684 (2017).

[19] 21.4% perovskite mini-module (19.32 cm²) (Microquanta, accessed: 2021). http://www.microquanta.com/en/newsinfo/80D096B5B598F211/.

[20] Oxford PV completes build-out of its Brandenburg factory (Oxford PV, accessed: 2021). https://www.oxfordpv.com/news/oxford-pv-completes-build-out-its-brandenburg-factory.

[21] Y. Jiang, S.-C. Yang, Q. Jeangros, S. Pisoni, T. Moser, S. Buecheler, A. N. Tiwari and F. Fu, Joule **4**, 1-17 (2020).

[22] N. K. Tailor, M. Abdi-Jalebi, V. Gupta, H. Hu, M. I. Dar, G. Li and S. Satapathi, J. Mater. Chem. A **8**, 21356-21386 (2020).

[23] C. Liu, Y.-B. Cheng and Z. Ge, Chem. Soc. Rev. **49**, 1653-1687 (2020).

[24] F.-Z. Qiu, M.-H. Li, J.-J. Qi, Y. Jiang and J.-S. Hu, Aggregate **2**, 66-83 (2021).

[25] Y. Jiang, E. J. Juarez-Perez, Q. Ge, S. Wang, M. R. Leyden, L.

K. Ono, S. R. Raga, J. Hu and Y. B. Qi, Mater. Horiz. **3**, 548-555 (2016).

[26] M. Remeika, S. R. Raga, S. Zhang and Y. B. Qi, J. Mater. Chem. A **5**, 5709-5718 (2017).

[27] N.-G. Park and K. Zhu, Nat. Rev. Mater. **5**, 333-350 (2020).

[28] A. T. Barrows, A. J. Pearson, C. K. Kwak, A. D. F. Dunbar, A. R. Buckley and D. G. Lidzey, Energy Environ. Sci. **7**, 2944-2950 (2014).

[29] Y. Deng, E. Peng, Y. Shao, Z. Xiao, Q. Dong and J. Huang, Energy Environ. Sci. **8**, 1544-1550 (2015).

[30] M. Yang, Z. Li, M. O. Reese, O. G. Reid, D. H. Kim, S. Siol, T. R. Klein, Y. Yan, J. J. Berry, M. F. A. M. v. Hest and K. Zhu, Nat. Energy **2**, 17038 (2017).

[31] K. Hwang, Y.-S. Jung, Y.-J. Heo, F. H. Scholes, S. E. Watkins, J. Subbiah, D. J. Jones, D.-Y. Kim and D. Vak, Adv. Mater. **27**, 1241-1247 (2015).

[32] Z. Yang, W. Zhang, S. Wu, H. Zhu, Z. Liu, Z. Liu, Z. Jiang, R. Chen, J. Zhou, Q. Lu, Z. Xiao, L. Shi, H. Chen, L. K. Ono, S. Zhang, Y. Zhang, Y. B. Qi, L. Han and W. Chen, Sci. Adv. **7**, eabg3749 (2021).

[33] M. Xiao, F. Huang, W. Huang, Y. Dkhissi, Y. Zhu, J. Etheridge, A. Gray-Weale, U. Bach, Y.-B. Cheng and L. Spiccia, Angew. Chem. Int. Ed. **126**, 10056-10061 (2014).

[34] N. J. Jeon, J. H. Noh, Y. C. Kim, W. S. Yang, S. Ryu and S. I. Seok, Nat. Mater. **13**, 897-903 (2014).

[35] Z. Xia, Q. Dong, C. Bi, Y. Shao, Y. Yuan and J. Huang, Adv. Mater. **26**, 6503-6509 (2014).

[36] W. Nie, H. Tsai, R. Asadpour, J.-C. Blancon, A. Neukirch, G. Gupta, J. J. Crochet, M. Chhowalla, S. Tretiak, M. A. Alam, H.-L. Wang and A. D. Mohite, Science **347**, 522-525 (2015).

[37] P. Luo, Z. Liu, W. Xia, C. Yuan, J. Chen and Y. Lu, ACS Appl. Mater. Interfaces **7**, 2708-2714 (2015).

[38] P. Luo, Z. Liu, W. Xia, C. Yuan, J. Cheng and Y. Lu, J. Mater. Chem. A **3**, 12443-12451 (2015).

[39] G. Li, J. Y. L. Ho, M. Wong and H.-S. Kwok, Phys. Status Solidi RRL **10**, 153-157 (2016).

[40] H.-S. Kim, C.-R. Lee, J.-H. Im, K.-B. Lee, T. Moehl, A. Marchioro, S.-J. Moon, R. Humphry-Baker, J.-H. Yum, J. E. Moser, M. Grätzel and N.-G. Park, Sci. Rep. **2**, 591 (2012).

[41] J. Burschka, N. Pellet, S.-J. Moon, R. Humphry-Baker, P. Gao, M. K. Nazeeruddin, M. Grätzel, Nature **499**, 316-319 (2013).

[42] H. Zhou, Q. Chen, G. Li, S. Luo, T.-B. Song, H.-S. Duan, Z. Hong, J. You, Y. Liu and Y. Yang, Science **345**, 542-546 (2014).

[43] W. S. Yang, J. H. Noh, N. J. Jeon, Y. C. Kim, S. Ryu, J. Seo and S. I. Seok, Science **348**, 1234-1237 (2015).

[44] Q. Jiang, Y. Zhao, X. Zhang, X. Yang, Y. Chen, Z. Chu, Q. Ye, X. Li, Z. Yin and J. You, Nat. Photonics **13**, 460-466 (2019).

[45] J. Jeong, M. Kim, J. Seo, H. Lu, P. Ahlawat, A. Mishra, Y. Yang, M. A. Hope, F. T. Eickemeyer, M. Kim, Y. J. Yoon, I. W. Choi, B. P. Darwich, S. J. Choi, Y. Jo, J. H. Lee, B. Walker, S. M. Zakeeruddin, L. Emsley, U. Rothlisberger, A. Hagfeldt, D. S. Kim, M. Grätzel and J. Y. Kim, Nature **592**, 381–385 (2021).

[46] C. Momblona, L. Gil-Escrig, E. Bandiello, E. M. Hutter, M. Sessolo, K. Lederer, J. Blochwitz-Nimoth and H. J. Bolink, Energy Environ. Sci. **9**, 3456-3463 (2016).

[47] J. Feng, Y. Jiao, H. Wang, X. Zhu, Y. Sun, M. Du, Y. Cao, D. Yang and S. F. Liu, Energy Environ. Sci. **14**, 3035-3043 (2021).

[48] Q. Chen, H. Zhou, Z. Hong, S. Luo, H.-S. Duan, H.-H. Wang, Y. Liu, G. Li and Y. Yang, J. Am. Chem. Soc. **136**, 622-625 (2014).

[49] Y. Li, J. K. Cooper, R. Buonsanti, C. Giannini, Y. Liu, F. M. Toma and I. D. Sharp, J. Phys. Chem. Lett. **6**, 493-499 (2015).

[50] Z. Liu, L. Qiu, E. J. Juarez-Perez, Z. Hawash, T. Kim, Y. Jiang, Z. Wu, S. R. Raga, L. K. Ono, S. F. Liu and Y. B. Qi, Nat. Commun. **9**, 3880 (2018).

[51] H. Lu, Y. Liu, P. Ahlawat, A. Mishra, W. R. Tress, F. T. Eickemeyer, Y. Yang, F. Fu, Z. Wang, C. Avalos, B. Carlsen, A. Agarwalla, X. Zhang, X. Li, Y. Zhan, S. M. Zakeeruddin, L. Emsley, U. Rothlisberger, L. Zheng, A. Hagfeldt and M. Graetzel, Science **370**, eabb8985 (2020).

[52] J. Seo, S. Park, Y. C. Kim, N. J. Jeon, J. H. Noh, S. C. Yoon and S. I. Seok, Energy Environ. Sci. **7**, 2642-2646 (2014).

[53] J. H. Heo, H. J. Han, D. Kim, T. K. Ahn and S. H. Im, Energy Environ. Sci. **8**, 1602-1608 (2015).

[54] J. H. Heo, M. H. Lee, M. H. Jang and S. H. Im, J. Mater. Chem. A **4**, 17636-17642 (2016).

[55] H. Chen, F. Ye, W. Tang, J. He, M. Yin, Y. Wang, F. Xie, E. Bi, X. Yang, M. Grätzel and L. Han, Nature **550**, 92-95 (2017).

[56] E. H. Jung, N. J. Jeon, E. Y. Park, C. S. Moon, T. J. Shin, T.-Y. Yang, J. H. Noh and J. Seo, Nature **567**, 511-515 (2019).

[57] Y. Deng, S. Xu, S. Chen, X. Xiao, J. Zhao and J. Huang, Nat. Energy **6**, 633-641 (2021).

[58] M. R. Leyden, Y. Jiang and Y. B. Qi, J. Mater. Chem. A **4**, 13125-13132 (2016).

[59] Y. Jiang, M. R. Leyden, L. Qiu, S. Wang, L. K. Ono, Z. Wu, E. J. Juarez-Perez and Y. B. Qi, Adv. Funct. Mater. **28**, 1703835 (2017).

[60] Y. Jiang, M. Remeika, Z. Hu, E. J. Juarez-Perez, L. Qiu, Z. Liu, T. Kim, L. K. Ono, D.-Y. Son, Z. Hawash, M. R. Leyden, Z. Wu, L. Meng, J. Hu and Y. B. Qi, Adv. Energy Mater. **9**, 1803047 (2019).

[61] J. Li, H. Wang, X. Y. Chin, H. A. Dewi, K. Vergeer, T. W. Goh, J. Wei, M. Lim, J. H. Lew, K. P. Loh, C. Soci, T. C. Sum, H. J. Bolink, N. Mathews, S. Mhaisalkar and A. Bruno, Joule **4**, 1035-1053 (2020).

[62] D. Prat, J. Hayler and A. Wells, Green Chem. **16**, 4546 (2014).

[63] M. Zhang, D. Xin, X. Zheng, Q. Chen and W.-H. Zhang, ACS Sustainable Chem. Eng. **8**, 13126-13138 (2020).

[64] L. K. Ono, M. R. Leyden, S. Wang and Y. B. Qi, J. Mater. Chem. A **4**, 6693–6713 (2016).

[65] J. A. vila, C. Momblona, P. P. Boix, M. Sessolo and H. J. Bolink, Joule **1**, 431-442 (2017).

[66] R. Swartwout, M. T. Hoerantner and V. Bulovic, Energy Environ. Mater. **2**, 119-145 (2019).

[67] S. Ullah, J. Wang, P. Yang, L. Liu, Y. Li, A.-U. Rehman, S.-E. Yang, T. Xia, H. Guo and Y. Chen, Solar RRL **5**, 2100172 (2021).

[68] T. D. Lee and A. U. Ebong, Renew. Sust. Energ. Rev. **70**, 1286-1297 (2017).

[69] J. d. Wild, A. Meijerink, J. K. Rath, W. G. J. H. M. v. Sark and R. E. I. Schropp, Sol. Energy Mater. Sol. Cells **94**, 1919-1922 (2010).

[70] A. Chirilă, P. Reinhard, F. Pianezzi, P. Bloesch, A. R. Uhl, C.

Fella, L. Kranz, D. Keller, C. Gretener, H. Hagendorfer, D. Jaeger, R. Erni, S. Nishiwaki, S. Buecheler and A. N. Tiwari, Nat. Mater. **12**, 1107-1111 (2013).

[71]M. Barbato, E. Artegiani, M. Bertoncello, M. Meneghini, N. Trivellin, E. Mantoan, A. Romeo, G. Mura, L. Ortolani and E. Zanoni, J. Phys. D: Appl. Phys. **54**, 333002 (2021).

[72]L. Qiu, S. He, Y. Jiang and Y. B. Qi, J. Mater. Chem. A **9**, 22759-22780 (2021).

[73]M. Era, T. Hattori, T. Taira and T. Tsutsui, Chem. Mater. **9**, 8-10 (1997).

[74]L. K. Ono, S. Wang, Y. Kato, S. R. Raga and Y. B. Qi, Energy Environ. Sci. **7**, 3989-3993 (2014).

[75]S. Wang, L. K. Ono, M. R. Leyden, Y. Kato, S. R. Raga, M. V. Lee and Y. B. Qi, J. Mater. Chem. A **3**, 14631-14641 (2015).

[76]L. Gil-Escrig, C. Dreessen, F. Palazon, Z. Hawash, E. Moons, S. Albrecht, M. Sessolo and H. J. Bolink, ACS Energy Lett. **6**, 827-836 (2021).

[77]A. M. Igual-Muñoz, J. Navarro-Alapont, C. Dreessen, F. Palazon, M. Sessolo and H. J. Bolink, Chem. Mater. **32**, 8641-8652 (2020).

[78]X. Zhu, D. Yang, R. Yang, B. Yang, Z. Yang, X. Ren, J. Zhang, J. Niu, J. Feng and S. F. Liu, Nanoscale **9**, 12316-12323 (2017).

[79]M. Roβ, S. Severin, M. B. Stutz, P. Wagner, H. Köbler, M. Favin-Lévêque, A. Al-Ashouri, P. Korb, P. Tockhorn, A. Abate, B. Stannowski, B. Rech and S. Albrecht, Adv. Energy Mater. **11**, 2101460 (2021).

[80]M.-G. La-Placa, D. Guo, L. n. Gil-Escrig, F. Palazon, M. Sessolo and H. J. Bolink, J. Mater. Chem. C **8**, 1902-1908 (2020).

[81]A. M. Igual-Muñoz, A. Castillo, C. Dreessen, P. P. Boix and H. J. Bolink, ACS Appl. Energy Mater. **3**, 2755-2761 (2020).

[82]C.-W. Chen, H.-W. Kang, S.-Y. Hsiao, P.-F. Yang, K.-M. Chiang and H.-W. Lin, Adv. Mater. **26**, 6647-6652 (2014).

[83]D. Yang, Z. Yang, W. Qin, Y. Zhang, S. F. Liu and C. Li, J. Mater. Chem. A **3**, 9401-9405 (2015).

[84]M.-C. Jung, S. R. Raga and Y. B. Qi, RSC Adv. **6**, 2819-2825 (2016).

[85]M. Kam, Y. Zhu, D. Zhang, L. Gu, J. Chen and Z. Fan, Solar RRL **3**, 1900050 (2019).

[86]O. Malinkiewicz, C. Roldán-Carmona, A. Soriano, E. Bandiello, L. Camacho, M. K. Nazeeruddin and H. J. Bolink, Adv. Energy Mater. **4**, 140034 (2014).

[87]G. Longo, C. Momblona, M.-G. La-Placa, L. n. Gil-Escrig, M. Sessolo and H. J. Bolink, ACS Energy Lett. **3**, 214-219 (2018).

[88]L. Gil-Escrig, C. Momblona, M.-G. La-Placa, P. P. Boix, M. Sessolo and H. J. Bolink, Adv. Energy Mater. **8**, 1703506 (2018).

[89]A. M. Igual-Muñoz, J. Ávila, P. P. Boix and H. J. Bolink, Solar RRL **4**, 1900283 (2020).

[90]D. Zhao, W. Ke, C. R. Gricea, A. J. Cimarolia, X. Tan, M. Yang, R. W. Collinsa, H. Zhang, K. Zhu and Y. Yan, Nano Energy **19**, 88-97 (2016).

[91]X. Liu, X. Tan, Z. Liu, B. Sun, J. Li, S. Xi, T. Shi and G. Liao, J. Power Sources **443**, 227269 (2019).

[92]W.-G. Choi, S. Na, C.-G. Park and T. Moon, Sol. Energy **178**, 56-60 (2019).

[93]J. Hua, X. Deng, C. Niu, F. Huang, Y. Peng, W. Li, Z. Ku and Y.-b. Cheng, RSC Adv. **10**, 8905-8909 (2020).

[94]M. R. Leyden, L. K. Ono, S. R. Raga, Y. Kato, S. Wang and Y. B. Qi, J. Mater. Chem. A **2**, 18742-18745 (2014).

[95]M. R. Leyden, M. V. Lee, S. R. Raga and Y. B. Qi, J. Mater. Chem. A **3**, 16097-16103 (2015).

[96]Y. Jiang, M. R. Leyden, L. Qiu, S. Wang, L. K. Ono, Z. Wu, E. J. Juarez-Perez and Y. B. Qi, Adv. Funct. Mater. **28**, 1703835 (2018).

[97]L. Qiu, S. He, Z. Liu, L. K. Ono, D.-Y. Son, Y. Liu, G. Tong and Y. B. Qi, J. Mater. Chem. A **8**, 23404-23412 (2020).

[98]M. M. Tavakoli, L. Gu, Y. Gao, C. Reckmeier, J. He, A. L. Rogach, Y. Yao and Z. Fan, Sci. Rep. **5**, 14083 (2015).

[99]L. Luo, Y. Zhang, N. Chai, X. Deng, J. Zhong, F. Huang, Y. Peng, Z. Ku and Y.-B. Cheng, J. Mater. Chem. A **6**, 21143-21148 (2018).

[100]X. Deng, J. Hua, F. Huang, Y. Peng, W. Li, Z. Ku and Y.-b. Cheng, Sustain. Energy Fuels **4**, 2491-2496 (2020).

[101]L. Luo, Z. Ku, W. Li, X. Zheng, X. Li, F. Huang, Y. Peng, L. Ding and Y.-B. Cheng, Sci. Bull. **66**, 962-964 (2021).

[102]C. Niu, C. Wang, G. Zhang, Q. Zhao, C. Fang, W. Li, F. Huang, Z. Ku and Y.-b. Cheng, Solar RRL **5**, 2100102 (2021).

[103]L. Qiu, S. He, Y. Jiang, D.-Y. Son, L. K. Ono, Z. Liu, T. Kim, T. Bouloumis, S. Kazaoui and Y. B. Qi, J. Mater. Chem. A **7**, 6920-6929 (2019).

[104]F. Sahli, N. Miaz, N. Salsi, C. Bucher, A. Schafflützel, Q. Guesnay, L. Duchêne, B. Niesen, C. Ballif and Q. Jeangros, ACS Appl. Energy Mater. **4**, 4333-4343 (2021).

[105]Q. Guo, C. Li, W. Qiao, S. Ma, F. Wang, B. Zhang, L. Hu, S. Dai and Z. a. Tan, Energy Environ. Sci. **9**, 1486-1494 (2016).

[106]E. Pérez-Gutiérrez, M. J. Percino, D. M. Montoya, D. Solis-Ibarra, M. Cerón and O. Barbosa-García, ACS Appl. Energy Mater. **1**, 3843-3849 (2018).

[107]E. Pérez-Gutiérrez, M. J. Percino, P. Santos, M. Cerón, P. Ceballos, D. M. Montoya, O. Barbosa-García and S. Thamotharan, Mater. Today Commun. **25**, 101384 (2020).

[108]A. Ioakeimidis, C. Christodoulou, M. Lux-Steiner and K. Fostiropoulos, J. Solid State Chem. **244**, 20-24 (2016).

[109]J. Yin, H. Qu, J. Cao, H. Tai, J. Li and N. Zheng, J. Mater. Chem. A **34**, 13203-13210 (2016).

[110]P. Luo, S. Zhou, Y. Zhou, W. Xia, L. Sun, J. Cheng, C. Xu and Y. Lu, ACS Appl. Mater. Interfaces **9**, 42708-42716 (2017).

[111]P. Luo, Y. Zhou, S. Zhou, Y. Lu, C. Xu, W. Xia and L. Sun, Chem. Eng. Sci. **343**, 146-154 (2018).

[112]T. Moser, K. Artuk, Y. Jiang, T. Feurer, E. Gilshtein, A. N. Tiwari and F. Fu, J. Mater. Chem. A **8**, 21973-21982 (2020).

[113]Q. Chen, H. Zhou, Z. Hong, S. Luo, H.-S. Duan, H.-H. Wang, Y. Liu, G. Li and Y. Yang, J. Am. Chem. Soc. **136**, 622-625 (2013).

[114]J. Chen, J. Xu, L. Xiao, B. Zhang, S. Dai and J. Yao, ACS Appl. Mater. Interfaces **9**, 2449-2458 (2017).

[115]S. Rafizadeh, K. Wienands, P. S. C. Schulze, A. J. Bett, L. C. Andreani, M. Hermle, S. Glunz and J. C. Goldschmidt, ACS Appl. Mater. Interfaces **11**, 722–729 (2019).

[116]W. Soltanpoor, C. Dreessen, M. C. Sahiner, I. Susic, A. Z.

Afshord, V. S. Chirvony, P. P. Boix, G. Gunbas, S. Yerci and H. J. Bolink, ACS Appl. Energy Mater. **3**, 8257-8265 (2020).

[117] R. K. Kothandaraman, Y. Jiang, T. Feurer, A. N. Tiwari and F. Fu, Small Methods **4**, 2000395 (2020).

[118] T. Todorov, T. Gershon, O. Gunawan, Y. S. Lee, C. Sturdevant, L.-Y. Chang and S. Guha, Adv. Energy Mater. **5**, 1500799 (2015).

[119] Y. Jiang, T. Feurer, R. Carron, G. T. Sevilla, T. Moser, S. Pisoni, R. Erni, M. D. Rossell, M. Ochoa, R. Hertwig, A. N. Tiwari and F. Fu, ACS Nano **14**, 7502–7512 (2020).

[120] Y. Jiang and Y. B. Qi, Mater. Chem. Front. **5**, 4833-4850 (2021).

[121] Q. Han, Y.-T. Hsieh, L. Meng, J.-L. Wu, P. Sun, E.-P. Yao, S.-Y. Chang, S.-H. Bae, T. Kato, V. Bermudez and Y. Yang, Science **361**, 904-908 (2018).

[122] F. Sahli, J. Werner, B. A. Kamino, M. Bräuninger, R. Monnard, B. Paviet-Salomon, L. Barraud, L. Ding, J. J. D. Leon, D. Sacchetto, G. Cattaneo, M. Despeisse, M. Boccard, S. Nicolay, Q. Jeangros, B. Niesen and C. Ballif, Nat. Mater. **17**, 820-826 (2018).

[123] Z. Zhou, Z. Wang, Y. Zhou, S. Pang, D. Wang, H. Xu, Z. Liu, N. P. Padture and G. Cui, Angew. Chem. Int. Ed. **54**, 9705-9709 (2015).

[124] Y. Zong, Y. Zhou, M. Ju, H. F. Garces, A. R. Krause, F. Ji, G. Cui, X. C. Zeng, N. P. Padture and S. Pang, Angew. Chem. Int. Ed. **55**, 14723-14727 (2016).

[125] S. Pang, Y. Zhou, Z. Wang, M. Yang, A. R. Krause, Z. Zhou, K. Zhu, N. P. Padture and G. Cui, J. Am. Chem. Soc. **138**, 750-753 (2016).

[126] Y. Chang, L. Wang, J. Zhang, Z. Zhou, C. Li, B. Chen, L. Etgar, G. Cui and S. Pang, J. Mater. Chem. A **5**, 4803-4808 (2017).

[127] S. R. Raga, L. K. Ono and Y. B. Qi, J. Mater. Chem. A **4**, 2494-2500 (2016).

[128] S. R. Raga, Y. Jiang, L. K. Ono and Y. B. Qi, Energy Technol. **5**, 1750-1761 (2017).

[129] Z. Li, M. Yang, J.-S. Park, S.-H. Wei, J. J. Berry and K. Zhu, Chem. Mater. **28**, 284-292 (2015).

[130] T. Zhang, N. Guo, G. Li, X. Qian, L. Lia and Y. Zhao, J. Mater. Chem. A **4**, 3245-3248 (2016).

[131] H. Fan, F. Li, P. Wang, Z. Gu, J.-H. Huang, K.-J. Jiang, B. Guan, L.-M. Yang, X. Zhou and Y. Song, Nat. Commun. **11**, 5402 (2020).

[132] C. Mortan, T. Hellmann, M. Buchhorn, M. d. E. Melzi, O. Clemens, T. Mayer and W. Jaegermann, Energy Sci. Eng. **8**, 3165-3173 (2020).

[133] J. J. Yoo, G. Seo, M. R. Chua, T. G. Park, Y. Lu, F. Rotermund, Y.-K. Kim, C. S. Moon, N. J. Jeon, J.-P. Correa-Baena, V. Bulović, S. S. Shin, M. G. Bawendi and J. Seo, Nature **590**, 587-593 (2021).

[134] M.-H. Li, J.-Y. Shao, Y. Jiang, F.-Z. Qiu, S. Wang, J. Zhang, G. Han, J. Tang, F. Wang, Z. Wei, Y. Yi, Y.-W. Zhong and J.-S. Hu, Angew. Chem. Int. Ed. **60**, 16388-16393 (2021).

[135] F.-Z. Qiu, M.-H. Li, S. Wang, J.-Y. Sun, Y. Jiang, J.-J. Qi and J.-S. Hu, J. Mater. Chem. A **9**, 24064-24070 (2021).

[136] I. Levine, S. Gupta, A. Bera, D. Ceratti, G. Hodes, D. Cahen, D. Guo, T. J. Savenije, J. Ávila, H. J. Bolink, O. Millo, D. Azulay and I. Balberg, J. Appl. Phys. **124**, 103103 (2018).

[137] S. Wang, Y. Jiang, E. J. Juarez-Perez, L. K. Ono and Y. B. Qi, Nat. Energy **2**, 16195 (2017).

[138] E. J. Juarez-Perez, L. K. Ono, M. Maeda, Y. Jiang, Z. Hawash and Y. B. Qi, J. Mater. Chem. A **6**, 9604-9612 (2018).

[139] N. Li, S. Tao, Y. Chen, X. Niu, C. K. Onwudinanti, C. Hu, Z. Qiu, Z. Xu, G. Zheng, L. Wang, Y. Zhang, L. Li, H. Liu, Y. Lun, J. Hong, X. Wang, Y. Liu, H. Xie, Y. Gao, Y. Bai, S. Yang, G. Brocks, Q. Chen and H. Zhou, Nat. Energy **4**, 408-415 (2019).

[140] M. S. Abbas, S. Hussain, J. Zhang, B. Wang, C. Yang, Z. Wang, Z. Wei and R. Ahmad, Sustain. Energy Fuels **4**, 324-330 (2020).

[141] G. Yang, Z. Ren, K. Liu, M. Qin, W. Deng, H. Zhang, H. Wang, J. Liang, F. Ye, Q. Liang, H. Yin, Y. Chen, Y. Zhuang, S. Li, B. Gao, J. Wang, T. Shi, X. Wang, X. Lu, H. Wu, J. Hou, D. Lei, S. K. So, Y. Yang, G. Fang and G. Li, Nat. Photonics **15**, 681-689 (2021).

[142] Z. Song, C. L. McElvany, A. B. Phillips, I. Celik, P. W. Krantz, S. C. Watthage, G. K. Liyanage, D. A. andM. J. Heben, Energy Environ. Sci. **10**, 1297-1305 (2017).

[143] M. V. Khenkin, E. A. Katz, A. Abate, G. Bardizza, J. J. Berry, C. Brabec, F. Brunetti, V. Bulović, Q. Burlingame, A. D. Carlo, R. Cheacharoen, Y.-B. Cheng, A. Colsmann, S. Cros, K. Domanski, M. Dusza, C. J. Fell, S. R. Forrest, Y. Galagan, D. D. Girolamo, M. Grätzel, A. Hagfeldt, E. v. Hauff, H. Hoppe, J. Kettle, H. Köbler, M. S. Leite, S. F. Liu, Y.-L. Loo, J. M. Luther, C.-Q. Ma, M. Madsen, M. Manceau, M. Matheron, M. McGehee, R. Meitzner, M. K. Nazeeruddin, A. F. Nogueira, Ç. Odabaşı, A. Osherov, N.-G. Park, M. O. Reese, F. D. Rossi, M. Saliba, U. S. Schubert, H. J. Snaith, S. D. Stranks, W. Tress, P. A. Troshin, V. Turkovic, S. Veenstra, I. Visoly-Fisher, A. Walsh, T. Watson, H. Xie, R. Yıldırım, S. M. Zakeeruddin, K. Zhu and M. Lira-Cantu, Nat. Energy **5**, 35-49 (2020).